Mineralia Slovaca, Web ISSN 1338-3523, ISSN 0369-2086, https://doi.org/10.56623/ms.2026.58.1.1
58, 1 (2026), 3 – 36,

Badenian-Pannonian (Langhian-Tortonian) evolution of the Blatné sub-basin, northwestern Danube Basin (Central Paratethys): integrated biostratigraphic, facies and seismic evidence from the Špačince-4 and Dubové-2 wells

SAMUEL RYBÁR[1, 2], NATÁLIA HUDÁČKOVÁ[1,*], ĽUBOMÍR SLIVA[4], MICHAL JAMRICH[1], KATARÍNA ŠARINOVÁ[3], MARIANNA KOVÁČOVÁ[1], ANDREJ RUMAN[1] and BRANISLAV ŠÁLY[4]

[1] Comenius University Bratislava, Faculty of Natural Sciences, Department of Geology and Paleontology, Ilkovičova 6, Mlynská dolina, 842 15 Bratislava, Slovak Republic

[2] Faculty of Mining and Geology, Department of Geodesy and Mine Surveying, Technical University of Ostrava, 17. listopadu 2172/15, 708 00 Ostrava, Poruba, Czech Republic

[3] Comenius University Bratislava, Faculty of Natural Sciences, Mlynská Dolina, Department of Mineralogy, Petrology and Economic Geology, Ilkovičova 6, 842 15 Bratislava, Slovak Republic

[4] NAFTA, a. s., 900 68 Plavecký Štvrtok, Slovak Republic

* Corresponding author: natalia.hudackova@uniba.sk

Abstract: The Špačince-4 and Dubové-2 wells in the Blatné sub-basin of the Danube Basin were integrated with SP/RT logs and seismic profiles to refine Badenian-Pannonian (Langhian-Tortonian) stratigraphy and basin evolution. The study integrates core-facies, provenance, XRF, well-log and seismic interpretations with reinterpreted data from, in total, 29 foraminiferal, 41 calcareous-nannofossil and 16 palynological samples. Calcareous nannofossils document NN4–NN6 zones, while planktonic foraminifera constrain parts of the succession to CPN7–CPN8. Key markers include *Orbulina suturalis, Globorotalia bykovae, Sphenolithus heteromorphus, ?Helicosphaera ampliaperta* and *Reticulofenestra pseudoumbilicus > 7 µm*. The succession is mainly lower to upper Badenian, whereas Sarmatian-Pannonian deposits are inferred from upper log-defined and seismic intervals. The Špačince-4 borehole records basal coarse-clastic and volcaniclastic deposits passing upward into marine gravity-flow and suspension-dominated facies; Dubové-2 preserves a thinner marine succession above pre-Neogene basement. Agglutinated morphogroups are locally compatible with bathyal-equivalent conditions where preservation permits, while *Bulimina-Bolivina-Uvigerina*-rich assemblages are consistent with enhanced organic flux and locally reduced oxygen availability. Phytoclast-rich residues indicate terrestrial input. Seismic data reveal an asymmetric half-graben bounded by listric normal faults above a low-angle detachment, with Badenian growth strata overlain by Sarmatian onlap and subhorizontal Pannonian post-rift deposits. Overall, the succession records Badenian syn-rift sedimentation followed by Sarmatian-Pannonian shallowing and deltaic-lacustrine-fluvial infilling.

Key words: Neogene, Central Paratethys, biostratigraphy, sedimentology, core analysis

Introduction

The Miocene evolution of the northwestern Central Paratethys was controlled by back-arc extension associated with the Alpine-Carpathian orogenic system and the lateral extrusion of the ALCAPA mega-unit (Royden et al., 1983; Tari et al., 1992; Schmid et al., 2008). Within this framework, the Pannonian Basin System developed as a series of syn-rift depocentres characterized by rapid subsidence, high sedimentation rates (e.g. Balázs et al., 2016), and coeval volcanic activity during the Middle Miocene (Harangi et al., 2025). The Danube Basin represents one of the principal depocentres of this system (Sztanó et al., 2016). Its northwestern sector, including the Blatné sub-basin, preserves a thick Miocene succession recording the transition from syn-rift extension to post-rift thermal subsidence (Šujan et al., 2021; Rybár et al., 2025). The regional extensional evolution of the Danube

Basin, including its Middle Miocene back-arc setting, polyphase rifting and subsequent post-rift subsidence, is well established (Hók et al., 2016; Šujan et al., 2021, 2026). Previous studies also place the initial opening of the Blatné sub-basin in the lower Badenian and continued syn-rift subsidence in the upper Badenian (Šarinová et al., 2018, 2021; Rybár & Kotulová, 2023; Rybár et al., 2024, 2025). However, the local expression of this regional evolution within individual fault blocks of the Blatné sub-basin remains incompletely constrained. In particular, uncertainties concern: (1) the position and local expression of the transition from proximal coarse-clastic and volcaniclastic sedimentation to unequivocally marine deposition; and (2) the lateral correlation and fault-block-scale architecture of Badenian gravity-flow packages between the studied wells and adjacent parts of the sub-basin. This study therefore aims to refine the local chronostratigraphic and tectono-sedimentary architecture of the Blatné sub-basin rather than to revise the established regional extensional model. To address these issues, this study presents an integrated investigation of the Špačince-4 (Lat: 48°26'19.6794"N; Lon: 17°37'40.2977"E) and Dubové-2 (Lat: 48°29’20.9416"N; Lon: 17°35'52.6196"E) deep wells in the Blatné sub-basin. An unpublished technical report by Hudáčková et al. (2018) presented the original foraminiferal, calcareous-nannofossil and palynological datasets, together with preliminary core-lithology, SP/RT logs and palaeoenvironmental interpretations. In the present study, these data were reinterpreted, and selected archived residues and slides were re-examined where clarification or revision was required. The study further integrates substantially expanded core-facies and provenance analyses, new XRF measurements and new reflection-seismic interpretation. Its principal contribution is the integration of the two well successions within a fault-block-scale model of the Blatné half-graben. Published numerical ages and data from neighbouring wells were used for regional chronostratigraphic calibration; no new radiometric dating was performed.

The objectives were to: (1) refine the biostratigraphic framework of the Miocene succession using multiple microfossil groups; (2) reconstruct depositional environments and facies architecture from the core data; (3) correlate the studied well successions using SP and RT logs and integrate them with the reflection-seismic profiles; and (4) determine whether the contrasting Špačince-4 and Dubové-2 successions reflect different structural positions within the fault-controlled Blatné half-graben (Fig. 1).

Geological setting

Tectonic framework

The Danube Basin forms the northwestern segment of the Pannonian Basin System (PBS), a Miocene back-arc basin that developed during extensional collapse of the Alpine-Carpathian orogen (Royden et al., 1982, 1983; Horváth et al., 2006, 2015; Matenco & Radivojević, 2012; Tari et al., 1992, 2021). Basin formation was controlled by slab rollback beneath the Carpathian arc and lateral extrusion of the ALCAPA mega-unit (Ratschbacher et al., 1991a, b; Schmid et al., 2008). The basin evolved through a four-stage rifting process (Šujan et al., 2021) corresponding to: (1) lower Badenian (Langhian), (2) upper Badenian (lower Serravallian), (3) Sarmatian (upper Serravallian), and (4) lower Pannonian (Tortonian). Thermal subsidence prevailed from the mid–upper Pannonian onward, while basin inversion likely began in the Pliocene and continues today (Royden et al., 1983; Horváth, 1995; Balázs et al., 2016, 2021; Šujan et al., 2016, 2021). The Danube Basin trends NE–SW, is ~200 km long and ~100 km wide, and is bounded by the Eastern Alps (W), Central Western Carpathians (N), and the Transdanubian Range (SE) (Vass, 2002; Sztanó et al., 2016). The Hurbanovo-Diósjenő Fault Zone represents a major tectonic boundary within the southeastern sector (Klučiar et al., 2016).

Basement structure

The pre-Neogene basement of the Danube Basin consists predominantly of Paleozoic crystalline basement rocks of the Tatric and Veporic units with their late Paleozoic to Mesozoic sedimentary cover (Fusán et al., 1987; Droppa et al., 2024). In the northern sector, these are overlain by Fatric and Hronic Mesozoic nappe units (Biely et al., 1996; Hók et al., 2014). The northwestern margin locally preserves remnants of the Central Carpathian Paleogene Basin (Biela, 1978). South of the Hurbanovo-Diósjenő Fault Zone, the basement includes Paleozoic and Mesozoic sedimentary units of the Transcarpathian Central Range (Fusán et al., 1987) and locally Paleogene sediments (Tari et al., 1993; Sztanó & Tari, 1993). The structural framework reflects Late Cretaceous nappe stacking which was later reactivated during Miocene back-arc extension (Hók et al., 2014; Konečný et al., 2002).

Syn-rift evolution and sub-basin development

The Slovak part of the basin comprises several Miocene sub-basins, including the Blatné, Želiezovce, Rišňovce, Komjatice, and Gabčíkovo-Győr sub-basins (Vass, 2002; Šujan et al., 2021; Rybár et al., 2024). The cumulative Neogene sedimentary fill locally exceeds 8 km in the Gabčíkovo-Győr sub-basin, although this total includes deposits accumulated during syn-rift and post-rift stages (Killényi & Šefara, 1989; Hrušecký, 1999; Šujan et al., 2021; Rybár et al., 2024). By contrast, the approximately 3-km-thick fill of the Blatné sub-basin is largely represented by Badenian deposits associated with the first two syn-rift phases (Csibri et al., 2018; Šujan et al., 2021; Rybár et al., 2025).

Lower Badenian (Langhian) interval

Rifting initiated in the Blatné and Želiezovce sub-basins during the lower Badenian (Šarinová et al., 2018, 2021; Rybár & Kotulová, 2023; Rybár et al., 2025). This stage coincided with marine transgression of the Central Paratethys (e.g. Popov et al., 2004) and deposition of mudstones, sandstones, and volcanogenic sediments of the Špačince Formation (Biela, 1978; Vass, 2002; Rybár et al., 2016). Volcanic activity in the Danube Basin before approximately 14.1 Ma is documented by $^{40}Ar/^{39}Ar$ dating (Rybár et al., 2024). The Middle Miocene volcanic flare-up preceded and accompanied the Langhian/Serravallian sea-level fall (~13.8 Ma) and was dominated by high-K calc-alkaline magmatism (Karátson et al., 2000, 2007; Lexa et al., 2010; Chernyshev et al., 2013; Šarinová et al., 2021; Rybár et al., 2025; Lexa et al., 2025).

Upper Badenian (lower Serravallian) interval

Rifting continued during the upper Badenian, increasing accommodation space, particularly in the Blatné sub-basin (Rybár & Kotulová, 2023; Rybár et al., 2025). Sedimentation included mudstones and sandy density-flow deposits of the Báhoň and Pozba formations (Vass, 2002; Šujan et al., 2021).

Sarmatian (upper Serravallian) interval

Major basin expansion occurred during the Sarmatian, particularly in the northern and central sub-basins (Šujan et al., 2021; Rybár et al., 2024). Sedimentation shifted toward restricted marine, brackish, and freshwater environments, reflected in the Vráble and Ripňany formations (Fordinál & Elečko, 2000). Calc-alkaline volcanism persisted into the Sarmatian and was followed by smaller-volume alkaline magmatism (Harangi et al., 1995; Wijbrans et al., 2007; Harangi & Lenkey, 2007; Pécskay et al., 2006; Seghedi & Downes, 2011; Chernyshev et al., 2013; Sant et al., 2020; Nováková et al., 2020), reflecting progressive lithospheric thinning (Lexa et al., 2010).

Pannonian (Tortonian)

The lower Pannonian marks the final syn-rift phase and transition to thermal post-rift subsidence (Šujan et al., 2021). Deep-basin mudstones and gravity sediments of

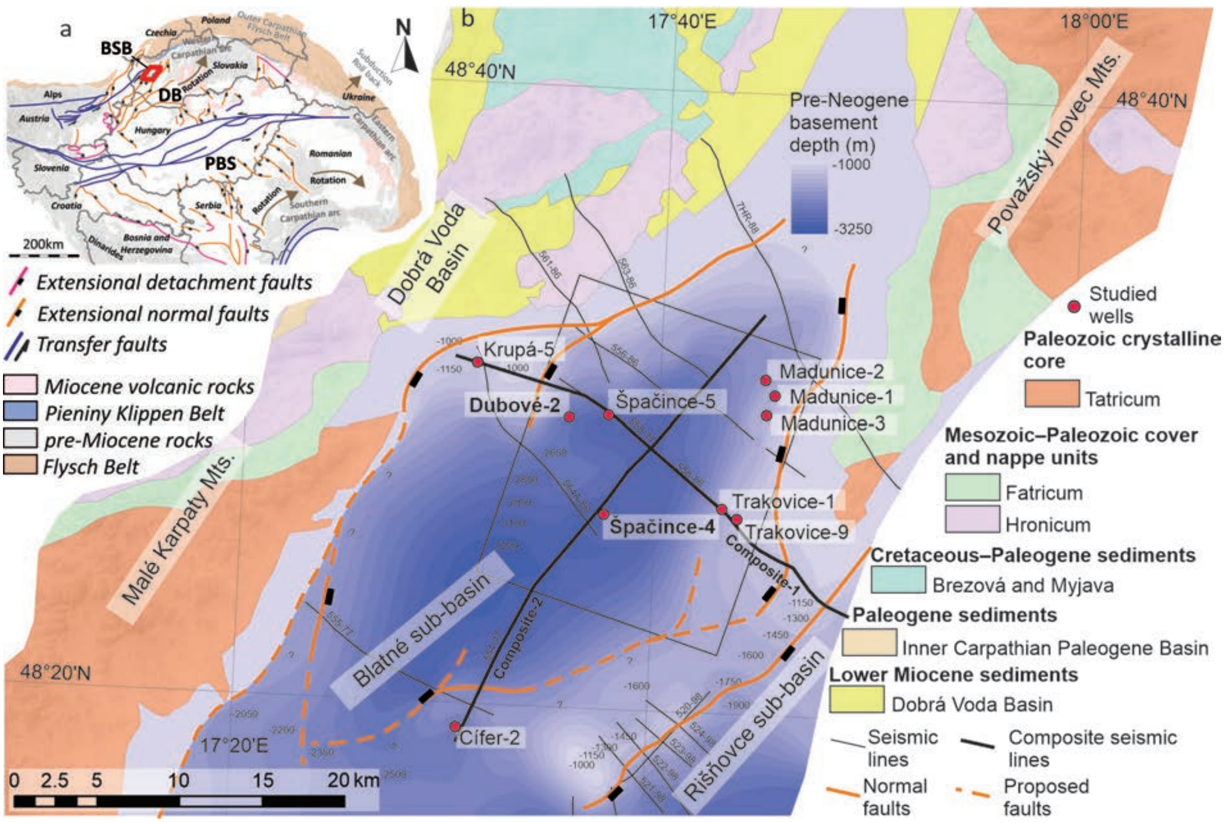

Fig. 1. (a) Location of the Blatné sub-basin (BSB) within the Danube Basin (DB) and Pannonian Basin System (PBS), modified from Fodor et al. (2021). (b) Locations of the studied and referenced wells and reflection-seismic profiles, modified from Šarinová et al. (2021).

the Ivanka Formation were followed by deltaic (Beladice Fm.) and fluvial-lacustrine deposits (Volkovce Fm.) (Vass, 2002; Sztanó et al., 2016).

Post-rift subsidence dominated during the upper Pannonian (upper Tortonian–Messinian) (Royden et al., 1983; Horváth, 1995), and basin inversion since ~6–5 Ma resulted in erosion at basin margins and subsequent deposition of Plio-Pleistocene sediments (Šujan et al., 2016, 2018).

Materials and Methods

Core material and framework

The well-core material from the Špačince-4 and Dubové-2 deep wells was obtained from the NAFTA, a. s., repository in Gbely (Slovakia). Well-core preparation, sedimentological description, micropalaeontological analyses, and palaeoecological interpretation were conducted at the Department of Geology and Paleontology, Comenius University in Bratislava. All samples and slides are archived in the departmental collection and at NAFTA, a. s. The study integrates sedimentological core analysis, well-log and seismic interpretation, and multiproxy micropalaeontological investigation to reconstruct depositional environments and refine the biostratigraphic framework of the Blatné sub-basin (Fig. 1).

Data sources and provenance

The micropalaeontological dataset comprises 29 foraminiferal, 41 calcareous-nannofossil and 16 palynological samples originally processed and analysed for the unpublished technical report of Hudáčková et al. (2018). That report also included preliminary lithological descriptions, SP/RT-log observations and palaeoenvironmental interpretations of the Špačince-4 and Dubové-2 wells. In the present study, the original dataset was reinterpreted using updated taxonomic, biostratigraphic and palaeoecological frameworks. Selected archived residues and slides were also re-examined where clarification or revision of individual identifications was required. New work includes substantially expanded core-facies description and imaging, handheld-XRF analysis of the Špačince-4 succession, and reflection-seismic interpretation. The new thin-section data and existing SP/RT logs were re-evaluated and integrated with these new datasets. Published numerical

Tab. 1
Summary of datasets used in this study

Dataset	Špačince-4	Dubové-2	Origin and use
Foraminifera	15 samples	14 samples	Hudáčková et al. (2018); reinterpreted and partly re-examined
Calcareous nannofossils	22 samples, 998–3,098 m	19 samples, 1,501–2,707 m	Hudáčková et al. (2018); reinterpreted and partly re-examined
Palynology	12 samples	4 samples	Hudáčková et al. (2018); qualitative reinterpretation
Sedimentological cores	28 spot cores; 52.2 m recovered, 1,190–3,348 m	23 spot cores; 89.9 m recovered, 1,501–2,751 m	Expanded core description and facies interpretation
Thin sections	6 samples	1 at a depth of 1,705 m	Existing petrographic data re-evaluated in this study
XRF	160 samples from 31 intervals, 697–3,347 m	None	New semiquantitative handheld-XRF dataset
SP and RT logs	Available	Available	Legacy data reinterpreted and correlated with core data
Seismic data	Four legacy 2D line segments combined into two composite profiles		New seismic-stratigraphic interpretation
Numerical ages	Published regional age constraints		Used for calibration only; no new radiometric dating

Note to Tab. 1. The wells were sampled by discontinuous spot coring; the stated depth ranges represent the distribution of examined cores and not continuously recovered intervals.
Detailed sample depths, core identifiers, analytical metadata and the distribution of the 16 palynological samples between the two wells are provided in Supplementary Tab. S1.

ages and results from neighbouring wells were used for regional correlation. No new radioisotopic dating was undertaken (Tab. 1).

Sedimentology and subsurface data interpretation

Sedimentological and petrographic analysis

Preliminary lithological descriptions were provided by Hudáčková et al. (2018). In this study, the cores were re-examined in substantially greater sedimentological detail, focusing on lithofacies, depositional processes and sediment provenance. The dataset comprised 28 discontinuous spot cores from Špačince-4 (C6–C32 and C34), representing 52.2 m of recovered material from intervals between 1,190 and 3,348 m, and 23 spot cores from Dubové-2 (C1–C23), representing 89.9 m between 1,501 and 2,751 m. Core samples were cut perpendicular to bedding, washed, stabilized with a dispersive adhesive where necessary, and then photographed, scanned and digitized. Lithofacies were defined from grain size, sorting, matrix or clast support, clast composition, bed contacts, grading, lamination, ripple structures, intraclasts, soft-sediment deformation, bioturbation and fossil content. Depositional processes were interpreted from combinations of these criteria, following Boggs (2006), Nichols (2009), Talling et al. (2012), Patruno et al. (2015), Rossi et al. (2017) and Pellegrini et al. (2020). Intervals lacking direct core control were interpreted from SP/RT-log motifs and seismic character and are therefore considered lower-confidence interpretations. The observed criteria, facies associations, depositional interpretations, chronostratigraphic assignments and confidence levels for both wells are summarized in Tabs. 4 and 5.

Petrographic analysis was based on seven thin sections: six from Špačince-4 – C34 at 3,347–3,348 m, C32 at 3,257–3,259 m, C30a at 3,158–3,159.3 m, C24 at 2,848–2,850 m, C18 at 2,405–2,408 m and C17 at 2,298–2,303 m – and one from Dubové-2 at ~1,705 m. The sections were examined qualitatively under transmitted and cross-polarized light to identify volcanic, carbonate, sedimentary and metamorphic components and assess changes in sediment provenance. Because no modal point counting was performed, the compositional results are treated as qualitative.

Well-log data and correlation

Spontaneous-potential (SP) and resistivity (RT) logs were examined for the Špačince-4 and Dubové-2 wells. These digitized legacy records were supplied by NAFTA, a. s.; no additional paper-to-digital conversion was performed. SP is expressed in millivolts and RT in Ω m. The working dataset did not specify the original vertical sampling or digitization interval, or any pre-processing, filtering or depth adjustments applied before delivery. Relevant technical metadata are retained in the legacy documentation and digital repository of NAFTA, a. s. Regional lithological correlation and log-motif interpretation followed Emery and Myers (1996) and Rider and Kennedy (2011). Funnel-shaped motifs indicate sustained upward coarsening, bell-shaped motifs upward fining, symmetrical motifs paired coarsening- and fining-upward trends, and serrated motifs irregular high-frequency fluctuations without a persistent trend. Motifs were identified from the relative shapes of the SP and RT curves and their departures from local baselines, rather than from universal numerical thresholds (Rider & Kennedy, 2011). Log responses were calibrated locally against the discontinuous core record by matching recovered intervals to the corresponding curves and comparing log motifs with observed grain-size trends, lithofacies and vertical facies arrangements. Because spot coring and core recovery were discontinuous, calibration could not be applied throughout either well; interpretations based solely on log character are therefore considered tentative and assigned lower confidence than those supported directly by core observations.

Seismic interpretation and well ties

Four legacy 2D seismic line segments were assembled into two composite profiles: Composite 1 combines lines 558_77, 558_86 and 558a_86, whereas Composite 2 comprises line 554_77. The data are archived in the digital repository of NAFTA, a. s., were used with the company's permission, and were imported, displayed and interpreted in Petrel. The accompanying spatial metadata specify the Pulkovo 1942 / Gauss-Krüger Zone 3N coordinate reference system (EPSG:28463). SEG-Y header inspection indicated a nominal trace spacing of approximately 25 m and a record length of about 6 s two-way travel time for all lines. Line 554_77 contains 1,246 traces with 3,000 samples per trace at a 2 ms sampling interval and is approximately 31.2 km long. Lines 558_77, 558_86 and 558a_86 contain 515, 194 and 176 traces, respectively, each with 1,500 samples per trace at a 4 ms interval; their approximate lengths are 12.9, 4.8 and 4.4 km. Seismic amplitudes were stored as 32-bit IEEE floating-point values. Because the original acquisition and processing parameters, including frequency content, were unavailable, vertical resolution was assessed qualitatively and no bed-scale interpretation was attempted. Interpretation followed sequence- and seismic-stratigraphic principles outlined by Mitchum and Vail (1977) and Fischer and Veeken (2015). Horizons were identified from laterally traceable reflections, changes in amplitude, continuity and configuration, and systematic reflection terminations. Faults were recognized from reflector offsets and terminations, abrupt changes in dip or continuity, and associated deformation and growth geometries. Onlap and downlap were identified from systematic updip and downdip reflection terminations, respectively. Growth strata were defined as wedge-shaped packages that thicken toward faults, locally display fanning reflectors and show upward changes in fault displacement (Mitchum & Vail, 1977; Fischer & Veeken, 2015). Composite 1 was constrained by lithological and well-log data from the Kr-5, Du-2, Sp-5, Tra-1 and Tra-9 wells, whereas Composite 2 was constrained by the Ci-2 and Šp-4 wells (Fig. 1). Available check-shot time-depth relationships were used to convert well-log and lithological markers from depth to two-way travel time before seismic correlation. The underlying check-shot and sonic data are retained by NAFTA, a. s., and may be made available on reasonable request, subject to the data owner's permission. Interpretive confidence is highest near well ties and along laterally continuous, clearly expressed reflections. It decreases with distance from well control, across joins between legacy line segments, and within intervals containing weak, discontinuous or structurally complex reflections. Stratigraphic assignments and depositional interpretations in these areas are therefore considered tentative.

X-ray fluorescence analysis

A total of 160 homogenized core samples from 31 discontinuous intervals in the Špačince-4 well, spanning 697.08–3,347.30 m, were analysed on 31 August and 1 September 2022 using a handheld BRUKER TITAN S1 600 X-ray fluorescence analyser with GeoMining calibration. The instrument reported 48 major- and trace-element variables and an analytical total in percent; values below the detection threshold were recorded as "< LOD". The analytical report does not specify numerical detection limits, measurement uncertainty, replicate quality-control analyses, matrix-matched reference-standard results, measurement duration or further details of sample preparation. The data are therefore treated as semiquantitative and used to assess relative downhole compositional variations rather than exact absolute concentrations. The complete dataset is provided in Appendix 3 and summarized in Supplementary Table S1.

Micropalaeontology

The micropalaeontological dataset comprises 15 quantitative foraminiferal samples and 22 calcareous-nannofossil samples from Špačince-4, and 14 quantitative foraminiferal samples and 19 calcareous-nannofossil samples from Dubové-2, together with 16 palynological samples: 12 from Špačince-4 and four from Dubové-2. These samples were originally analysed for Hudáčková et al. (2018). For the present study, the results were reinterpreted, and selected archived residues and slides were re-examined to clarify or revise individual taxonomic identifications, biozonal assignments and palaeoecological interpretations. Sample depths and analytical status are listed in Supplementary Tab. S1.

Foraminifera

Approximately 100 g of sediment per sample was treated with hydrogen peroxide and wet-sieved through 0.071 and 1 mm meshes. Residues were examined using an Olympus SZ75 stereomicroscope and a polarizing microscope, and selected specimens were imaged with a QUANTA FEG 250 SEM (Appendix 1). Where possible, residues were split to obtain approximately 300 identifiable specimens; when fewer were available, all recovered specimens were recorded and used cautiously, mainly for taxonomic and biostratigraphic interpretation. Taxonomy follows Loeblich and Tappan (1992), Cicha et al. (1998) and Holbourn et al. (2013). Palaeoecological interpretation follows Boltovskoy (1976), Boltovskoy and Wright (1976), Murray (2006), and Murray and Alve (2011); agglutinated morphogroups follow Murray et al. (2011), palaeodepth estimates follow Murray (2006), Hohenegger (2005), and taphonomic assessment follows Holcová (1997). Water-depth interpretations were treated as indicative and were applied only where assemblages were sufficiently preserved and plausibly in situ. Benthic assemblages were evaluated jointly with food supply and organic flux, oxygen availability, substrate and sedimentological context. Assemblages affected by dissolution, mould preservation, selective preservation, sorting or reworking were not treated as direct depth indicators. Interpretations were based on the proportional composition of ecological groups and morphogroups, visualized using POLPAL (Nalepka & Walanus, 2003), and supplemented by the chemical data in Appendix 3. Relative abundances of the palaeoecological groups were calculated as percentages of the total benthic-foraminiferal assemblage, whereas agglutinated morphogroup abundances were calculated as percentages of the total agglutinated-foraminiferal assemblage. Samples with fewer than 30 identifiable specimens were excluded from percentage-based palaeoecological and morphogroup analyses. Samples without foraminifera were classified as barren, whereas assemblages dominated by moulds, dissolved tests or mechanically damaged specimens were classified as poorly preserved. Photodocumentation was performed using an TESCAN SEM at the Department of Geology and Paleontology, Faculty of Sciences, Comenius University.

Calcareous nannofossils

Nannofossils were prepared using smear-slide and decantation techniques following Bown (1998). Slides were mounted using Norland 61 adhesive and examined under an Olympus BX50 polarized-light microscope at 1,250× magnification. Photodocumentation was performed using an Olympus Infinity 2 camera with QuickPHOTO CAMERA 2.3 and ScopeImage 9.0 software. No fixed-count protocol was applied. Slides were examined systematically for taxonomic composition, preservation, reworked taxa, biostratigraphic markers and zonal assignment. The resulting qualitative to semiquantitative sample-by-sample observations are provided in Appendix 4. Taxonomy follows Young (1998) and Young et al. (2022).

Palynology

Approximately 20 g of sediment per sample was processed using cold HF and HCl to remove silicates and carbonates. Heavy liquid separation ($ZnCl_2$, density 2 g/cm^3) concentrated organic residues containing pollen, spores, and other palynomorphs. Slides mounted in glycerine were examined using a Zeiss Axioscope microscope (40× and 63×).

Chronostratigraphic framework

Correlation between the Central Paratethys regional stages and the Mediterranean scale follows Piller et al. (2007), Kováč et al. (2007), Hohenegger (2014) and Wade et al. (2011). Stratigraphically significant taxa were used to constrain depositional timing and relate sedimentation to tectonic phases and sea-level changes. No direct geochronological analyses were conducted on material from the Špačince-4 or Dubové-2 wells; all numerical ages used for correlation were derived from published studies of neighbouring wells and regional volcanic and sedimentary successions (e.g. Šarinová et al., 2021; Rybár et al., 2024).

The complete tables are provided with the manuscript as supplementary material. Tab. S1 lists the complete dataset inventory, including sample depths, core identifiers, analytical status and available methodological metadata. Appendices 1 and 2 provide species-by-sample foraminiferal data for Špačince-4 and Dubové-2, respectively. Appendix 3 contains the complete handheld-XRF dataset, including depths, reported variables, units and below-detection values, whereas Appendix 4 presents nannofossil sample identifiers, taxonomic inventories, preservation assessments, reworked taxa, biostratigraphic events and zonal assignments. Appendices 1–4 accompany the manuscript as supplementary material.

The principal methodological limitations are discontinuous core coverage, locally poor microfossil preservation, incomplete metadata for the legacy geophysical datasets and the semiquantitative nature of the handheld-XRF measurements. Interpretations based primarily on well logs, seismic geometry or regional correlation are therefore considered less certain than those supported directly by core and fossil evidence.

Results

Lithological description of the studied wells

Špačince-4 well

The deepest cored interval (3,356–3,320 m; Core/C34) consists of poorly sorted, matrix-supported carbonate conglomerate with angular clasts embedded in a black calcareous matrix (Fig. 2).

Core C33 at approximately 3,301–3,302 m was not available for direct examination, and borehole-log data are absent for this interval. Core C32 at 3,257–3,259 m contains a poorly sorted volcanic conglomerate composed predominantly of altered volcanic lithoclasts derived from intermediate volcanism, together with spherulitized vitroclasts. The non-volcanic components include granitoid, biotite paragneiss, shale, carbonate and chert fragments, and the groundmass is chloritized. Carbonized plant fragments are also present. Tectonically deformed mudstones and sandstones were reported from this depth by Gaža (1963). Both SP and RT logs display pronounced funnel-shaped trends (Fig. 2).

The interval 3,200–3,125 m (C31, 30) consists of a massive grey-green zeolitized crystal-vitric tuff, where glass shards were replaced by analcime. Two distinct excursions are visible on the SP log, and the RT log shows a low-amplitude bell-shaped trend.

The interval between 3,125 and 2,850 m (C28–C25) is dominated by dark grey heterolithic mudstone-siltstone with subordinate light grey siltstone to very fine sandstone beds. Bedding is mm–cm scale, with parallel to wavy lamination and sharp to irregular/wavy contacts. Mud-rich intervals are laminated to locally mottled/weak-moderately bioturbated. Silty to very fine sandy beds show local normal grading, massive to faintly laminated bases, parallel/ripple lamination, and thin mud drapes. Irregular, lobate, loaded, and contorted laminae indicate soft-sediment deformation and possible dewatering. The core is locally fractured. The SP log displays a serrated pattern with minor excursions, whereas the RT log shows symmetrical to bell-shaped excursions of higher amplitude (Fig. 2).

The interval between 2,848 and 2,850 m (C24) consists of a massive, granule-pebble conglomerate/breccia with poorly sorted angular to subrounded lithic clasts. Larger platy/tabular clasts, some internally laminated, likely represent ripped-up mudstone-siltstone intraclasts. Bedding, grading, tractional lamination, bioturbation, and clear imbrication are absent; fabric is chaotic to weakly organized (Fig. 2). The conglomerates differ significantly from the underlying volcanic sequence in terms of clast composition. The clast assemblage is dominated by sedimentary lithologies, including sandstones (some of Eocene–Oligocene age, as indicated by enclosed foraminifera), calpionellid and radiolarian biomicrites, and other carbonate rocks, accompanied by chert, granitoid, and quartz-mica schist clasts.

The interval 2,850–2,150 m (C23 to 16) consists of alternating laminated to wavy-laminated mudstone-siltstone, massive to normally graded sandstone/pebbly sandstone, and matrix-rich fine conglomerate. The composition of the conglomerates and sandstones indicates a renewed input from volcanic sources. Volcanic grains are associated with granitoid, mica-schist, carbonate, siltstone, and sandstone clasts. Marine fossils, including red-algae (lithothamnia) fragments, suggest redeposition from a shallow-marine environment. Upsection, the abundance of unstable grains decreases, whereas quartz becomes progressively more abundant. Conglomeratic and pebbly beds are poorly sorted and contain abundant angular to subrounded lithic clasts, including common platy mudstone-siltstone intraclasts/rafts up to ~10 cm. Contacts are sharp to locally erosive or irregular, with chaotic to weakly stratified fabric, local clast clustering, ripple lamination, and thin laminated intervals. Bioturbation is limited, and clear imbrication is absent (Fig. 2). Both SP and RT logs show serrated trends, with consistently high RT amplitudes.

The interval between 2,150 and 1,125 m (C15–C6) is dominated by brown, finely laminated mudstone-siltstone, with subordinate thin fine-sandstone and siltstone laminae. Lamination is mainly parallel to low-angle/wavy, with common mud drapes/stringers and bedding-parallel partings/fractures. Conglomeratic material, large intraclasts, clear grading, and strong bioturbation are absent to rare (Fig. 2). According to Gaža (1963) carbonized plant fragments and marine macrofaunal remains are present. The SP and RT logs remain serrated with low amplitudes throughout this interval.

Between 1,125–625 m (C5 to C1), no core was available for this study, although core material exists. This interval is characterized by higher-amplitude serrations on the SP log. Gaža (1963) reported the presence of carbonized plant fragments and marine macrofaunal remains.

The uppermost interval, 625–0 m, lacks core material and is defined by high-amplitude serrated RT trends and medium-amplitude serrated SP trends.

XRF description of the Špačince-4 well

To further constrain compositional changes within the succession, XRF analyses were performed on drill-core samples. The results demonstrate that the volcanic horizon at depths of 3,158 and 3,258 m is characterized by elevated relative values of Zr, U, Si, and K, whereas Ca concentrations are lower compared to the surrounding sediments. The highest relative Ca values correspond to the occurrence of carbonate conglomerates at depths of approximately 3,350 and 2,850 m. Additional Ca enrichment was recorded in core samples from depths of 3,010 and 3,050 m. The systematic decrease in S values above a depth of 905 m, approaching near-zero values, is also observed (Appendix 3).

Dubové-2 well

The interval 3,000–2,780 m (C31 to 24) consists of tectonically deformed shale, limestone, quartz arenite, sandstone, and conglomerate (Gaža, 1968). SP and RT logs display high-amplitude symmetrical to bell-shaped excursions.

Between 2,780 and 2,720 m (C23), grey massive, bioturbated sandstones occur. The SP log shows a symmetrical trend, while the RT log exhibits funnel and bell-shaped patterns. The sandstones are dominated by carbonate clasts, some of which are clearly epiclastic. Quartz, feldspar, mica, chert, siltstone, volcanic lithic fragments, glauconite and bioclasts are also present in a micritic matrix.

The interval between 2,720 and 2,535 m (C22–C16) consists of grey to black sandy mudstone and muddy siltstone, locally grading into very fine sandstone. Bedding is laminated to faintly wavy/ripple laminated, with local mud-rich streaks, elongate mudstone intraclasts, diffuse grading, and bioturbation. Minor soft-sediment deformation is present (Fig. 3). SP and RT logs are mainly serrated, with minor high-amplitude excursions.

The interval between 2,535 and 2,060 m (C15–C6) consists of dark grey to brown mudstone, sandy mudstone and muddy siltstone that are massive to faintly laminated and locally bioturbated. Thin-shelled bivalves and other micro- to macrofauna are present. Coarse-grained beds and clear traction structures are absent to rare; the core is locally fractured (Fig. 3). SP and RT logs remain serrated.

A pronounced high-amplitude symmetrical trend is visible on both logs between 2,060–1,975 m.

The interval 1,975–470 m (C5 to 1) consists of brown mudstone to muddy siltstone/fine sandstone, massive to finely/wavy laminated and locally bioturbated. Synsedimentary folding, bedding-parallel partings, and minor fractures occur locally. A thin section from the fine-grained conglomerate in core C3 at approximately 1,705 m was examined for provenance. Its composition is dominated by carbonate, quartzite, arenite, phyllite, chert, and quartz

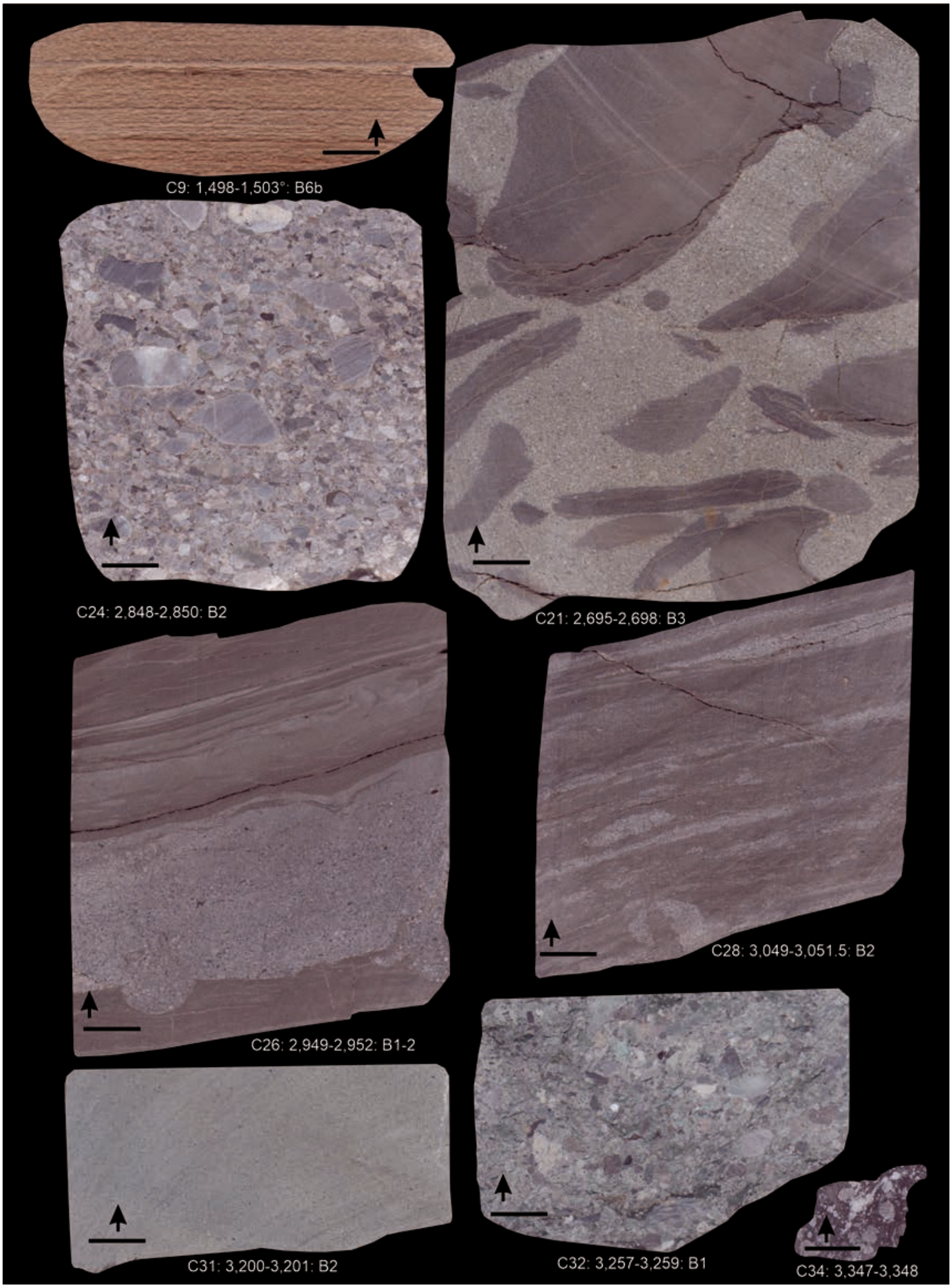

Fig. 2. Representative core slabs from the Špačince-4 well. Labels give core number, depth and box. The illustrated facies include basal paraconglomerate (C34), volcanic conglomerate (C32), zeolitized tuff (C31), heterolithic mudstone-siltstone and fine sandstone (C28 and C26), matrix-rich conglomerate and pebbly sandstone (C24 and C21), and laminated mudstone-siltstone (C9). Arrows indicate younging direction; 1 cm scale bars are shown in individual images.

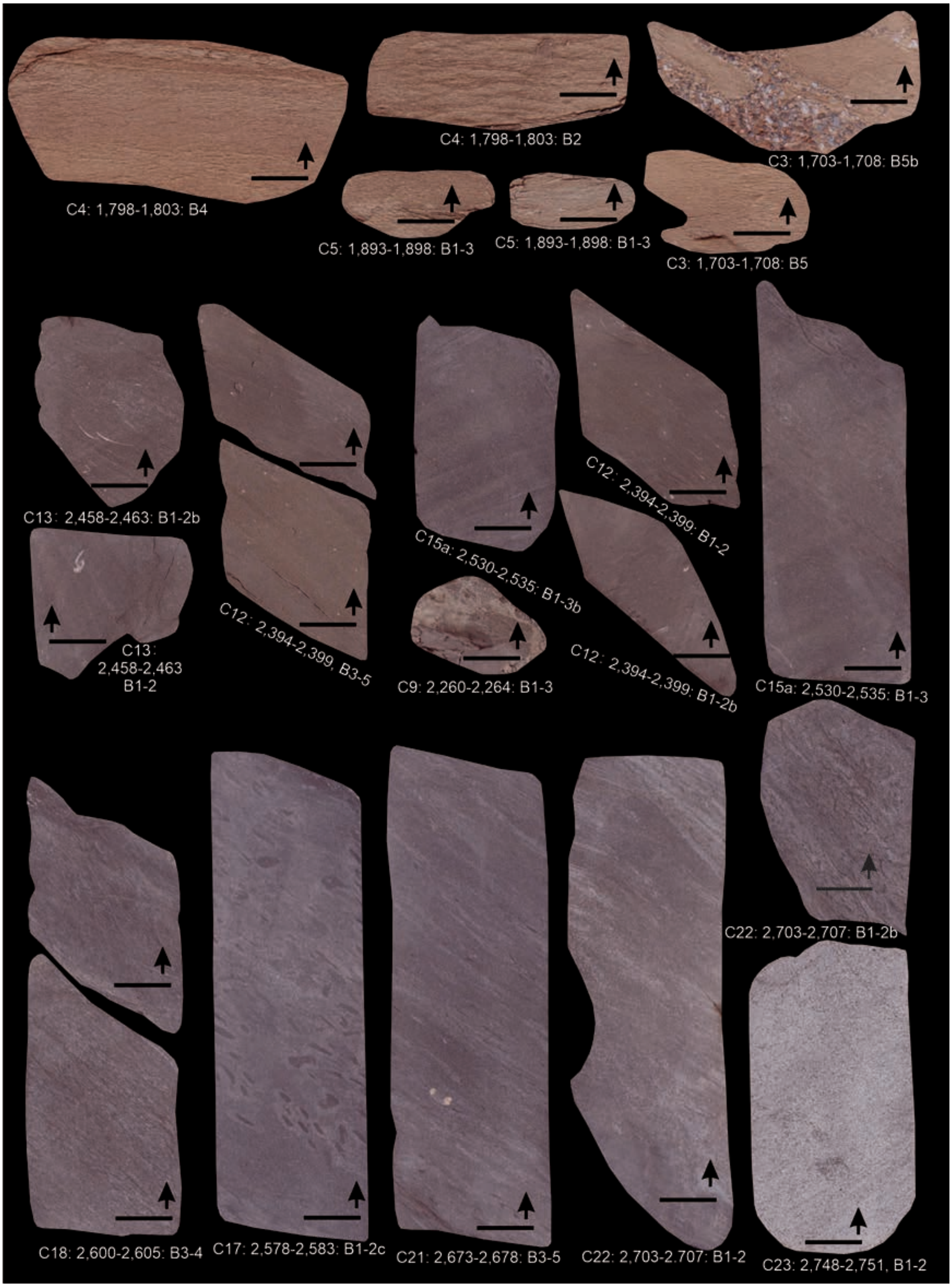

Fig. 3. Representative core slabs from the Dubové-2 well. Labels give core number, depth and box. The illustrated facies include bioturbated sandstone (C23), laminated sandy mudstone–muddy siltstone and fine sandstone (C22–C12), shell-rich reworked event beds (C9 and C3), and laminated muddy siltstone–fine sandstone (C5–C3). Arrows indicate younging direction; 1 cm scale bars are shown in individual images.

grains, whereas volcanic grains are rare. The conglomerate also contains bioclasts, including shell fragments, foraminifera, red algae, as well as the above-mentioned muddy intraclasts. Rare shell-rich paraconglomerate/bioclastic beds contain fragmented macrofossils and likely represent reworked event layers (Fig. 3). SP and RT logs display low-amplitude serrated trends.

Above 470 m, core material is absent. SP and RT logs display high-amplitude serrated to symmetrical excursions.

Between 80–0 m, excursions become more pronounced.

Biostratigraphy

The micropalaeontological results presented below are based on the dataset originally generated by Hudáčková et al. (2018), subsequently reinterpreted for the present study and supplemented by partial re-examination of selected archived residues and slides. The principal biostratigraphic events, zonal assignments, regional stages, formation correlations and confidence levels are summarized in Tabs. 2 and 3; complete sample-level data are provided in Appendices 1, 2 and 4 and Supplementary Tab. S1.

Špačince-4 well (Šp-4)

Biostratigraphically informative samples and events are summarized below and in Tab. 2; complete taxonomic, accessory-residue and sample-level data are provided in Appendices 1 and 4 and Supplementary Tab. S1.

Foraminiferal assemblages are generally poorly preserved, particularly in the deepest intervals of the well. In cores 29 and 28 (3,098–3,049 m), foraminifera are retained in open nomenclature, because only moulds were preserved, whereas the original shell material was dissolved or mechanically damaged by compaction. Agglutinated genera, mainly *Reophax, Bathysiphon, Haplophragmoide*s and *Saccammina*, dominate the assemblages, likely due to early diagenetic processes. Planktonic foraminifera are absent in core 28; therefore, the biostratigraphic interpretation is based on the benthic species *Saccammina grzybowskii*, whose first occurrence in the Badenian was reported by Cicha et al. (1998). Calcareous nannofossils from the same interval are represented by low-diversity and poorly preserved assemblages containing rare zonal markers *Sphenolithus heteromorphus* and *Helicosphaera walbersdorfensis*, indicating the ?NN4–NN5 nannofossil zones. Rare diatoms and silicoflagellates occur locally; their complete sample distribution is provided in Appendix 1.

Planktonic foraminifera from core 27 (3,002–3,004.5 m) are poorly preserved and commonly occur only as moulds. The first occurrence of the stratigraphically important species *Orbulina suturalis* (Fig. 4, item 1) was identified in core 26 at 2,949–2,952 m. The occurrence of *Sphenolithus heteromorphus* and *Helicosphaera waltrans* in cores 21 and 17, at 2,695–2,698 m and 2,298–2,303 m, respectively, indicates the NN5 Zone and a Langhian age.

The important biostratigraphic event was recognized in core 12 (1,798–1,804 m), where the acme of *Globorotalia bykovae* together with a bloom of small planktonic foraminifera indicates an Upper Badenian age following Gonera (2013). This interpretation is further supported by the benthic foraminiferal assemblage characterized by the occurrence of *Bolivina dilatata maxima* and the dominance of the genera *Bulimina* and *Bolivina*, in agreement with Cicha et al. (1998) and Kováčová & Hudáčková (2009). Nannofossil assemblages throughout most of the Šp-4 well are generally poorly preserved and of low diversity, apart from core 9 (1,503–1,498 m). In this interval, increased diversity was recorded, including *Coronocyclus nitescens*, *Orthorhabdus rioi* and *Sphenolithus abies*, together with frequent occurrence of *Reticulofenestra pseudoumbilicus* > 7 µm. According to Bartol (2009), this event represents an alternative marker for the NN5/NN6 zonal boundary. The core 9 (1,498–1,503 m) was likewise assigned to the upper Badenian.

Dubové-2 well (Du-2)

Biostratigraphically informative samples and events are summarized below and in Tab. 3; complete taxonomic, accessory-residue and sample-level data are provided in Appendices 2 and 4 and Supplementary Tab. S1.

The lowermost studied samples from core 22 (2,707–2,703 m) yielded abundant planktonic specimens of *Ciperoella ciperoensis*, suggesting a Karpatian to Lower Badenian age according to Cicha et al. (1998). In cores 18–16 (2,605–2,555 m), foraminiferal tests are generally poorly preserved, predominantly occurring as molds; therefore, many taxa remain indeterminable and are left in open nomenclature. Low-diversity and low-abundance calcareous nannofossil assemblages were documented in the interval 2,707–2,535 m. Rare and poorly preserved specimens of the stratigraphically important species ?*Helicosphaera ampliaperta* were identified in the interval 2,707–2,703 m, indicating the NN4 Zone. Due to the absence of planktonic foraminifera in cores 18–17 (2,605–2,555 m), the biostratigraphic interpretation of this interval remains uncertain.

The most abundant and diverse foraminiferal assemblage was identified in core 15a (2,535–2,530 m). The assemblage contains a small proportion of planktonic taxa dominated by indeterminate *Globigerina* species and rare *Ciperoella ciperoensis*, which does not allow more precise stratigraphic assignment. Within the benthic assemblage, the occurrence of *Uvigerina macrocarinata* and *Lenticulina echinata* represents an important stratigraphic marker supporting assignment to the lower Badenian, corresponding to the CPN7 Zone (Cicha et al., 1975). The occur-

Tab. 2
Biostratigraphic summary of the Špačince-4 well

Depth/core	Analysed sample	Foraminiferal markers	Nannofossil markers	CPN zone	NN zone	Regional stage	Formation	Confidence
3,098–3,049 m; C29–C28	29/1–2/20; 29/1–2/80; 28/2/10; 28/2/80	No reliable zonal marker; poorly preserved agglutinated and benthic assemblages	Rare *Sphenolithus heteromorphus* and *Helicosphaera walbersdorfensis*; some specimens questionable	Not assigned	?NN4–NN5	lower Badenian, Langhian; tentative	Špačince Fm.	**L–M:**
2,949–2,952 m; C26	26/1/60	*Orbulina suturalis, Saccammina grzybowskii, Dentoglobigerina altispira*	*Helicosphaera walbersdorfensis, H. carteri, Reticulofenestra pseudoumbilicus > 7 µm*	Not assigned	Not formally assigned	lower Badenian, Langhian	Špačince Fm.	**M–H:**
2,695–2,698 m; C21	21/1/90	Barren of diagnostic foraminifera	*S. heteromorphus* and *Helicosphaera waltrans*	Not assigned	NN5	lower Badenian, Langhian	Špačince Fm.	**H for NN zone:**
2,298–2,303 m; C17	17/2/X	Reworked *Cassigerinella chipolensis*; no reliable in-situ foraminiferal marker	*S. heteromorphus*; *H. waltrans* not confirmed	Not assigned	NN5	lower Badenian, Langhian	Špačince Fm.	**M:**
1,798–1,804 m; C12	12/1–2/X	Acme of *Globorotalia bykovae*; *Orbulina universa*; *Pappina neudorfensis*; *Bolivina dilatata*	*Coccolithus pelagicus* and ?*Calcidiscus pataecus*; no diagnostic zonal marker	Not formally assigned	Not assigned	upper Badenian, lower Serravallian	Báhoň/ Pozba formations	**M–H:**
1,498–1,503 m; C9	9/1/X; 9/5/X	*Turborotalita quinqueloba, Globigerina praebulloides, Bolivina dilatata brevis*	*S. heteromorphus, R. pseudoumbilicus >* 7 µm, *Coronocyclus nitescens, Orthorhabdus rioi, Sphenolithus abies*	Not assigned	NN6/?NN5; NN5/NN6 boundary interval	Upper Badenian, lower Serravallian	Báhoň/ Pozba formations	**M–H:**

Formation assignments are regional lithostratigraphic correlations and are not determined directly from the fossil assemblages. **H** – high confidence: concordant evidence from adequately preserved foraminiferal and nannofossil assemblages; **M** – moderate confidence: supported by one fossil group, rare markers or partly affected preservation; **L** – low/tentative confidence: questionable identification, poor preservation, reworking or dependence on regional correlation. “Not assigned” means that the available assemblage does not justify a formal zonal designation.

Fig. 4. SEM images of selected foraminifera from the Špačince-4 and Dubové-2 wells. 1 – *Orbulina suturalis* – Šp-4/26/1/60; 2 – *Globigerina regularis* – Du-2/14/1–2–3/x; 3 – *Globorotalia* sp. – Du-2/14/1–2–3/x; 4–5 – *Globorotalia bykovae* – Šp-4/12/1–2/x; 6 – *Cassigerinella chipolensis* – Šp-4/16/4/x; 7 – *Trilobatus quadrilobatus* – Du-2/14/1–2–3/x; 8 – *Globigerina* cf. *bulloides* – Du-2/14/1–2–3/x; 9 – *Globoturborotalita druryi* – Du-2/3/3/50; 10 – *Globigerinella obesa* – Du-2/16/1–2/x; 11 – *Ciperoella ciperoensis* – Du-2/22/1–2/x; 12 – *Trilobatus quadrilobatus* – Du-2/14/1–2–3/x; 13 – *Globigerina* cf. *bulloides* – Du-2/14/1–2–3/x; 14 – *Paraglo-borotalia nana* – Šp-4/12/1–2/x; 15 – *Globotruncana* sp. – Šp-4/16/5/x; 16 – *Spirosigmoilina tenuis* – Du-2/18/3–4/x; 17 – *Bolivina hebes* – Du-2/16/1–2/x; 18 – *Bolivina* cf. *hebes* – Du-2/22/1–2/x; 19 – *Bolivina dilatata* – Du-2/16/1–2/x; 20 – *Bulimina striata* – Šp-4/12/1–2/x; 21 – *Uvigerina macrocarinata* – Du-2/22/1–2/x; 22 – *Uvigerina venusta* – Du-2/14/1–2–3/x; 23 – *Uvigerina bononiensis* subsp. *primiformis* – Du-2/18/3–4/x; 24 – *Uvigerina semiornata* – Du-2/14/1–2–3/x; 25 – *Trifarina angulosa* – Du-2/14/1–2–3/x; 26 – *Bulimina elongata* – Šp-4/11a/2/x; 27 – *Stilostomella* sp. indet. – Du-2/22/1–2/x; 28 – *Ammonia parkinsoniana* – Šp-4/16/4/x; 29 – *Cibicidoides ungerianus* – Du-2/14/1–2–3/x; 30 – *Valvulineria complanata* – Du-2/14/1–2–3/x; 31 – *Hanzawaia boueana* – Du-2/14/1–2–3/x; 32 – *Ceratocancris hauerii* – Šp-4/26/1/60; 33 – *Hansenisca soldanii* – Du-2/14/1–2–3/x; 34 – *Sahulia conica* – Du-2/14/1–2–3/x; 35 – *Gaudryina megagranosa* – Du-2/22/1–2/x; 36 – *Quinqueloculina* sp. indet. – Du-2/18/3–4/x; 37 – *Bathysiphon taurinensis* – Šp-4/11a/2/x; 38 – *Ammobaculites agglutinans* – Du-2/14/1–2–3/x; 39 – *Rhizammina algaeformis* – Du-2/14/1–2–3/x; 40 – *Lagenammina atlantica* – Du-2/14/1–2–3/x; 41 – *Uvigerina* aff. *bononiensis* subsp. primiformis – Du-2/14/1–2–3/x.

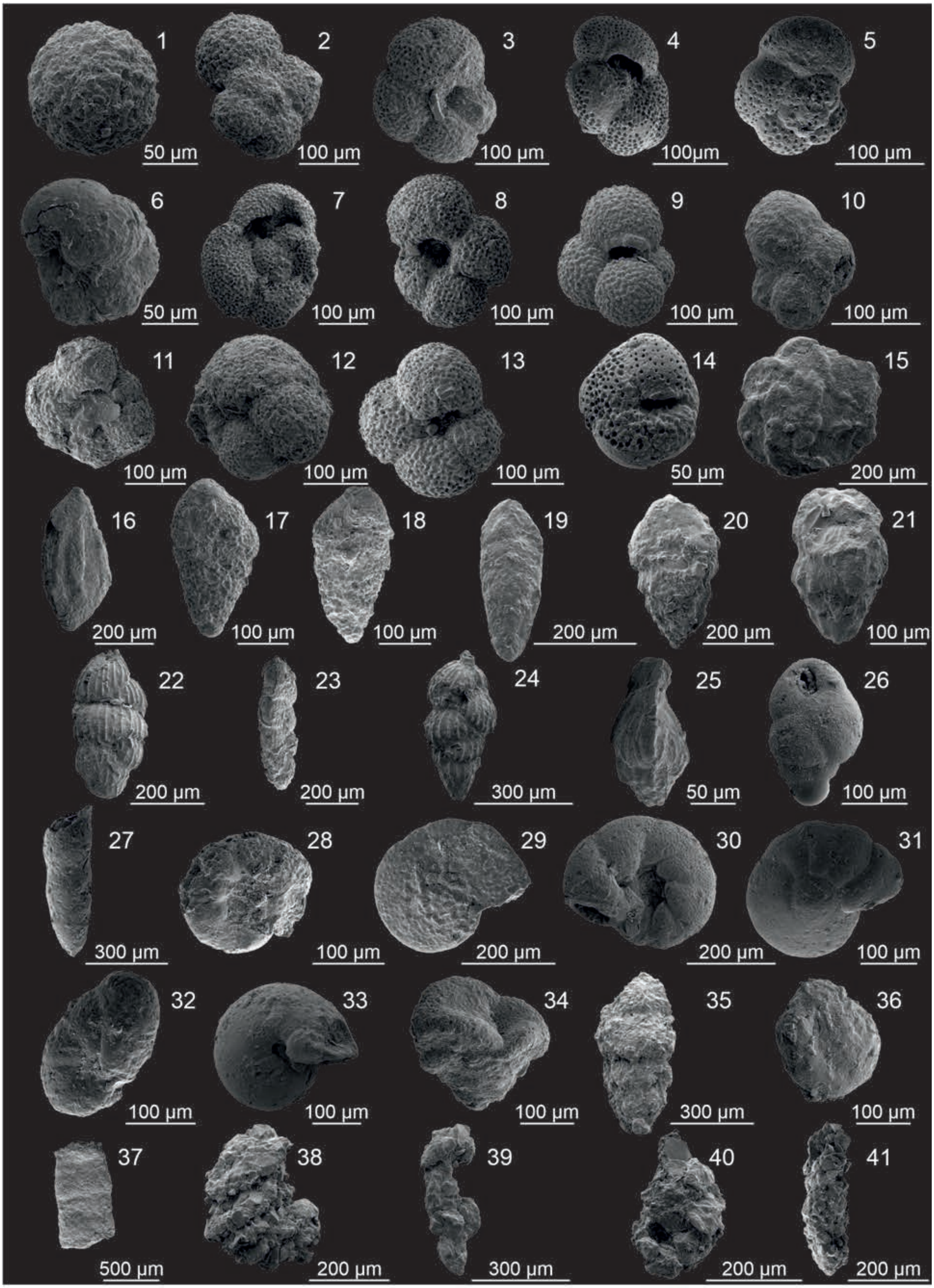
1
50 µm
2
100 µm
3
100 µm
4
100µm
5
100 µm
6
50 µm
7
100 µm
8
100 µm
9
100 µm
10
100 µm
11
100 µm
12
100 µm
13
100 µm
14
50 µm
15
200 µm
16
200 µm
17
100 µm
18
100 µm
19
200 µm
20
200 µm
21
100 µm
22
200 µm
23
200 µm
24
300 µm
25
50 µm
26
100 µm
27
300 µm
28
100 µm
29
200 µm
30
200 µm
31
100 µm
32
100 µm
33
100 µm
34
100 µm
35
300 µm
36
100 µm
37
500 µm
38
200 µm
39
300 µm
40
200 µm
41
200 µm

Tab. 3
Biostratigraphic summary of the Dubové-2 well

Depth/core	Analysed sample	Foraminiferal markers	Nannofossil markers	CPN zone	NN zone	Regional stage	Formation	Confidence	References
2,703–2,707 m; C22	22/1–2/XX	Reported *Ciperoella ciperoensis*; *Lenticulina* cf. *echinata*; *Bolivina dilatata*; *Bulimina striata*	?*Helicosphaera ampliaperta*	Not assigned	?NN4	Karpatian–lower Badenian; lower Badenian favoured regionally	Špačince Fm.	L–M:	*L. echinata* FO: Lagenidae Zone Grill (1943), CPN Cicha et al. (1975)
2,605–2,555 m; C18–C16	18/3–4/XX; 17/1–2/XX; 16/1–2/X	*Saccammina grzybowskii* in C18–C17; *Bolivina dilatata maxima* in C17; C16 poorly preserved	Mainly long-ranging *Coccolithus pelagicus*; *Reticulofenestra haqii* and associated taxa	CPN7 in C18–C17	Not assigned	lower Badenian, Langhian	Špačince Fm.	M:	*Saccammina grzybowskii* FO: Cicha et al. (1998)
2,530–2,535 m; C15a	15A/1–2–3/X	*Uvigerina macrocarinata*; *Lenticulina calcar*; rare *L. echinata*; reported *Ciperoella ciperoensis*	*Sphenolithus heteromorphus*; *Helicosphaera walbersdorfensis*; *Orthorhabdus serratus*	CPN7	NN5	lower Badenian, Langhian	Špačince Fm.	M–H:	*Uvigerina macrocarinata* FO: Cicha et al. (1975, 1998)
2,502–2,507 m; C14	14/1–2–3/X	*Pappina neudorfensis*; *Uvigerina bellicostata*; *Turborotalita quinqueloba*	*Helicosphaera walbersdorfensis*; *H. carteri*; *Reticulofenestra pseudoumbilicus*	CPN8	NN5	lower Badenian, Langhian; upper Badenian for Forams	Špačince Fm.	M–H:	*Pappina neudorfensis*, *Uvigerina bellicostata* – Bulimina/ Bolivina Zone, Upper Badenian (Steininger & Rögl, 1984; Haunold, 1995; Płonka, 1917)
1,703–1,708 m; C3	3/3/50; 3/5/50	Acme of *Globorotalia bykovae*‡; *Globoturborotalita druryi*; Bulimina-Bolivina acmes	*R. pseudoumbilicus* > 7 µm; *Coronocyclus nitescens* (circular)	CPN8	NN6	upper Badenian, lower Serravallian	Báhoň formations	M–H:	*Globoturborotalita druryi* – (NN6 Rybár et al., 2015; FO – 13,82 Ma Bojar et al., 2018)

Formation assignments are regional lithostratigraphic correlations and are not determined directly from the fossil assemblages. H – high confidence: concordant evidence from adequately preserved foraminiferal and nannofossil assemblages; M – moderate confidence: supported by one fossil group, rare markers or partly affected preservation; L – low/tentative confidence: questionable identification, poor preservation, reworking or dependence on regional correlation. “Not assigned” means that the available assemblage does not justify a formal zonal designation.

Fig. 5. Selected calcareous-nannofossil taxa and associated microfossils from the Špačince-4 and Dubové-2 wells. A – *Reticulofenestra minuta*, Šp-4, core 9; B – *Reticulofenestra haqii*, Du-2, core 9; C–D – *Reticulofenestra pseudoumbilicus*, Šp-4, core 9; E – *Coccolithus pelagicus*, Šp-4, core 21; F – *Cyclicargolithus floridanus*, Šp-4, core 9; G – *Coronocyclus nitescens*, Šp-4, core 9; H – *Braarudosphaera bigelowii*, Du-2, core 12; I – *Helicosphaera carteri*, Šp-4, core 9; J – *Helicosphaera waltrans*, Šp-4, core 21; K – *Helicosphaera walbersdorfensis*, Šp-4, core 9; L – *Sphenolithus heteromorphus*, Šp-4, core 17; M – *Orthorhabdus serratus*, Du-2, core 15; N – *Orthorhabdus rioi*, Du-2, core 17; O – *Umbilicosphaera rotula*, Šp-4, core 26; P – *Discoaster deflandrei*, Šp-4, core 29; Q – *Zygrhablithus bijugatus*, Šp-4, core 9; R – *Coccolithus eopelagicus*, Du-2, core 15; S – *Discoaster barbadiensis*, Du-2, core 10; T – *Tribrachiatus* orthostylus, Du-2, core 10; U – *Isthmolithus recurvus*, Šp-4, core 9; V – *Arkhangelskiella cymbiformis*, Du-2, core 17; W – *Eiffellithus turriseiffelii*, Du-2, core 22; X – *Eiffellithus eximius*, Du-2, core 15. Scale bars are 5 µm.

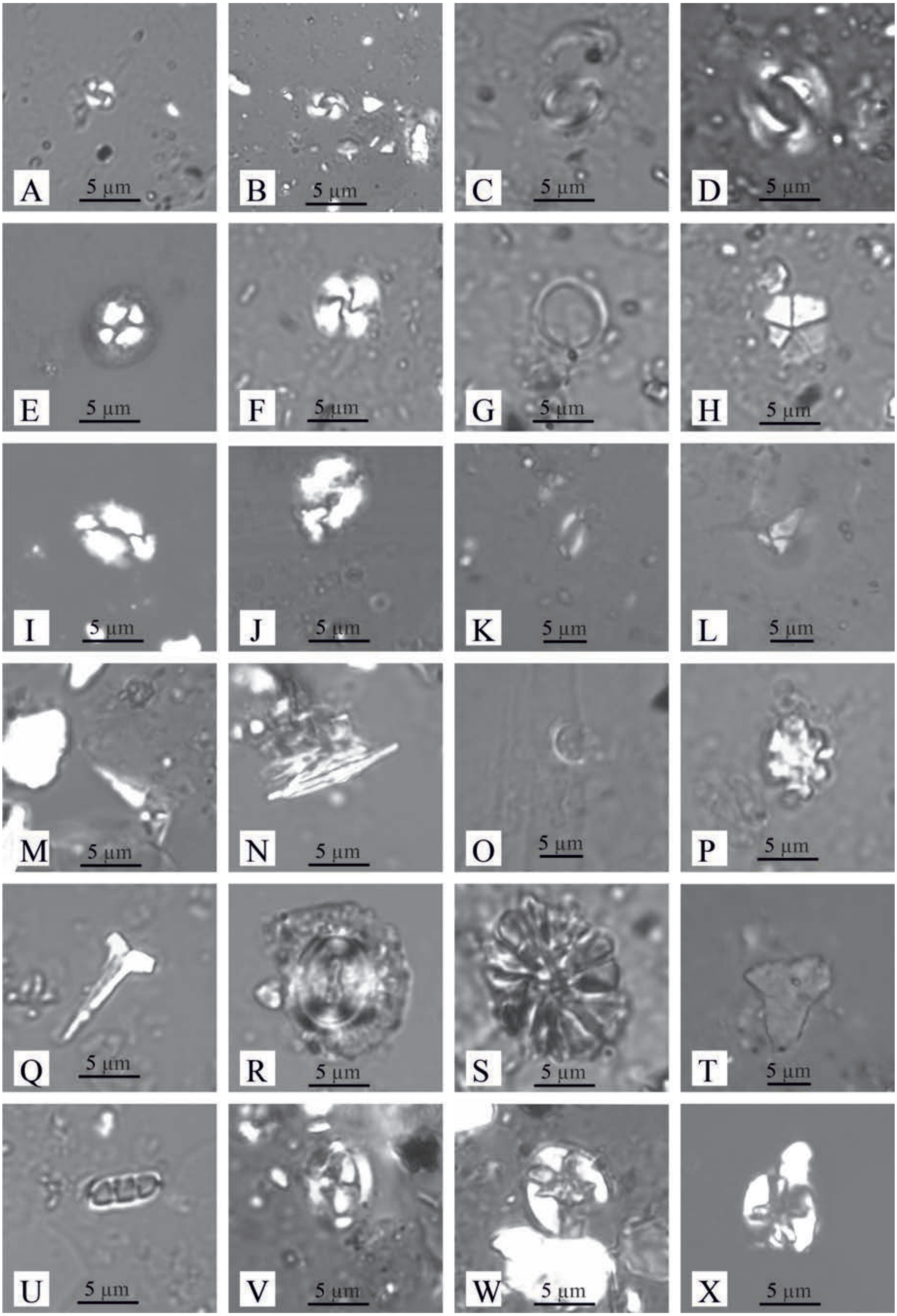
A
5 µm
B
5 µm
C
5 µm
D
5 µm
E
5 µm
F
5 µm
G
5 µm
H
5 µm
I
5 µm
J
5 µm
K
5 µm
L
5 µm
M
5 µm
N
5 µm
O
5 µm
P
5 µm
Q
5 µm
R
5 µm
S
5 µm
T
5 µm
U
5 µm
V
5 µm
W
5 µm
X
5 µm

rence of the zonal marker *Sphenolithus heteromorphus* in the interval 2,535–2,530 m indicates a Langhian age for the studied sediments. Another important stratigraphic event was identified in core 14 (2,507–2,502 m), where the occurrence of *Pappina neudorfensis* and *Uvigerina bellicostata*, together with a bloom of small *Turborotalita quinqueloba,* indicates an upper Badenian age, consistent with interpretations by Cicha et al. (1998) and Gonera (2013).

Assemblages from cores 5–1, particularly core 3 at 1,703–1,708 m, contain abundant *Globorotalia bykovae* and *Globoturborotalita druryi*, supporting the CPN8 Zone and an upper Badenian assignment (Cicha et al., 1998). The associated nannofossil assemblage, including *Reticulofenestra pseudoumbilicus > 7* µm and *Coronocyclus nitescens*, indicates the NN5/NN6 boundary interval. Comparable assemblages have previously been correlated with a broader late Badenian–Sarmatian interval, but the combined evidence used here favours an upper Badenian, lower Serravallian age. This interpretation is consistent with the results of Kováčová et al. (2009) and Rybár et al. (2015), who associated these assemblages with the NN6 Zone and a late Badenian–Sarmatian (Serravallian) age. Furthermore, the same interval yields a characteristic assemblage of the *Bulimina/Bolivina* Zone described by Grill (1941).

Pollen

Špačince-4 and Dubové-2 wells

All studied samples contain approximately 90 % phytoclasts, including plant tissues, dispersed gymnosperm cuticles and unidentified plant-derived particles, together with highly corroded pollen grains, mainly Pinaceae. Sporomorph preservation is very poor. Most phytoclasts show moderate to high maturity and some may be reworked; angular particles in at least half of the assemblage suggest short, rapid transport.

Paleoecology of Foraminifera

Špačince-4 well

Agglutinated taxa dominate the interval between 3,056 and 2,901.5 m. Considering that benthic foraminiferal assemblages may be significantly affected by taphonomic processes such as dissolution and dilution, while agglutinated assemblages are generally more resistant and remain better preserved, the relative abundances of agglutinated morphogroups were evaluated for palaeoecological interpretation following Murray et al. (2011). Morphogroup distributions in the intervals 3,056–2,901.5 m, 2,801.5–2,406 m and 1,897–1,700 m are compatible with upper-bathyal to outer-shelf ecological affinities only where the assemblages are reasonably preserved and plausibly in situ. The occurrence of shallow-water epiphytic taxa, together with evidence of dissolution, selective preservation and possible gravity-flow redeposition, reduces confidence in direct palaeodepth estimates. The C1-dominated assemblage at 1,498.5 m and the increasing abundance of epiphytic taxa at 1,082.5–799 m are consistent with shallowing, although changes in substrate, food supply and oxygenation may also have influenced the assemblages.

Calcareous assemblages between 2,598 and 2,406 m and between 1,412 and 1,082.5 m contain taxa tolerant of elevated organic flux and reduced oxygen availability. The change from high-productivity taxa at 2,598 m, through a mixed assemblage at 2,588 m, to low-oxygen-tolerant taxa at 2,406 m is consistent with increasing organic loading and/or decreasing oxygen availability, but does not independently demonstrate bottom-water dysoxia. These assemblages are therefore used to infer relative changes in organic supply and bottom- or pore-water oxygenation rather than direct water depth or a quantified redox state. Samples containing only agglutinated forms or clear evidence of reworking, including those at 2,405, 2297 and 698 m, are not used for confident palaeodepth or redox reconstruction.

Dubové-2 well

Foraminiferal tests are generally poorly preserved, indicating partial dissolution and alteration of the original assemblages. More resistant agglutinated taxa dominate the intervals between 2,531 and 2,212 m and occur again at 1,704 m (Fig. 7).

Morphogroup proportions based on Murray et al. (2011) show a predominance of morphogroup C1 in the lower and upper parts of the well. The assemblage at 2,601–2,577 m is compatible with a middle-bathyal ecological affinity only if it is reasonably in situ; poor preservation, dissolution and sorting reduce the confidence of this interpretation. The associated hyaline taxa and low proportion of epiphytic oligotrophic forms are consistent with enhanced organic flux and reduced oxygen availability at the sediment–water interface and/or within pore waters, but do not independently demonstrate the presence of an Oxygen Minimum Zone (OMZ). The B3- and C1-dominated assemblages at 2,556–2,531 m are compatible with a broad outer-shelf affinity. The sample at 1,791 m is not used as a direct depth indicator because sorting probably modified the original assemblage. The upward increase in shallow-water and epiphytic components is consistent with progressive shallowing, although changes in substrate, nutrient supply and oxygenation cannot be excluded as contributing controls (Fig. 7).

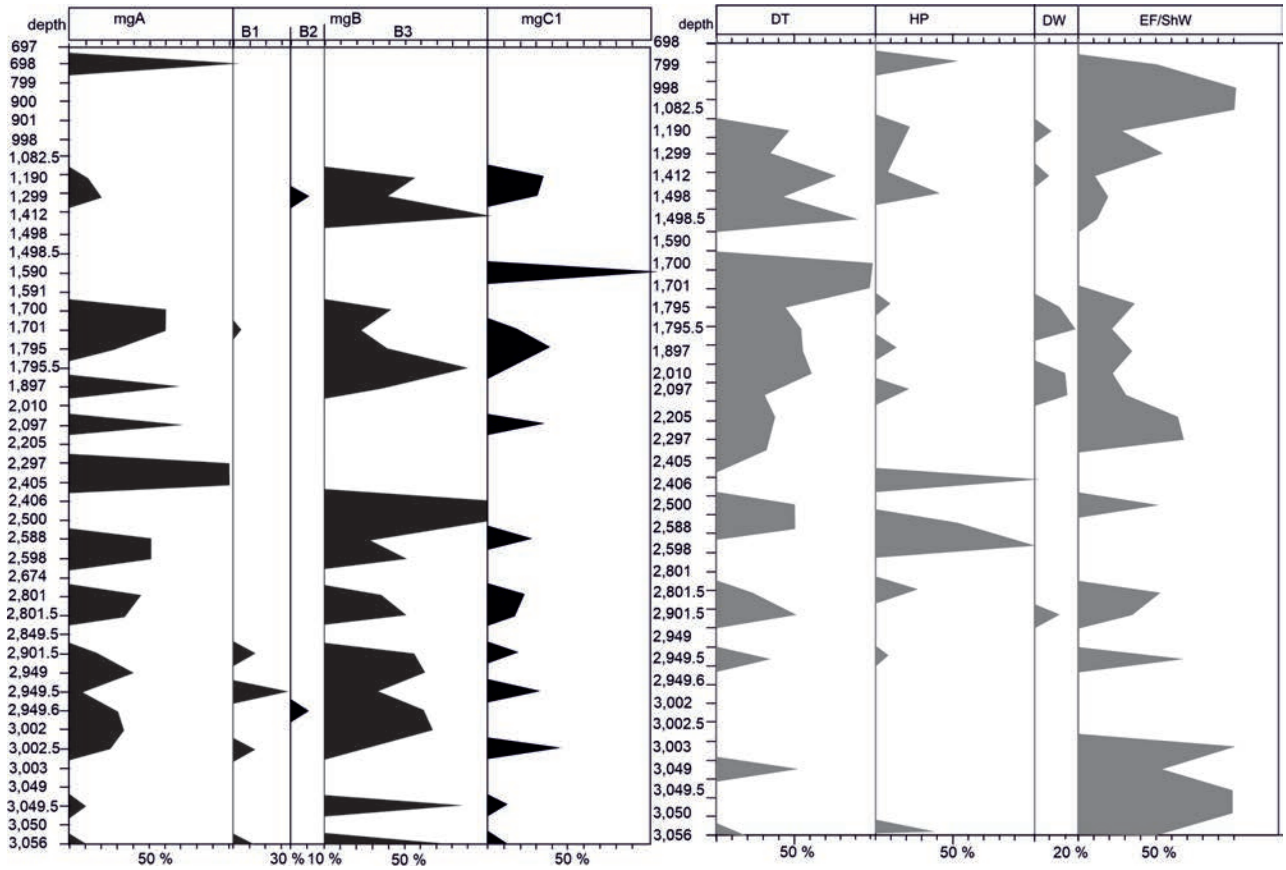

Fig. 6. Relative abundances of palaeoecologically significant benthic-foraminiferal groups in the Špačince-4 well. (Left side) Morphogroups of agglutinated foraminifera adapted from Murray et al. (2011). (Right side) palaeoecological groups of benthic foraminifera based on Murray (2006) and other authors. Abbreviations: HP – high productivity; DT – dysoxia-tolerant taxa; DW – deep-water taxa; EF/ShW – epifaunal/shallow-water taxa.

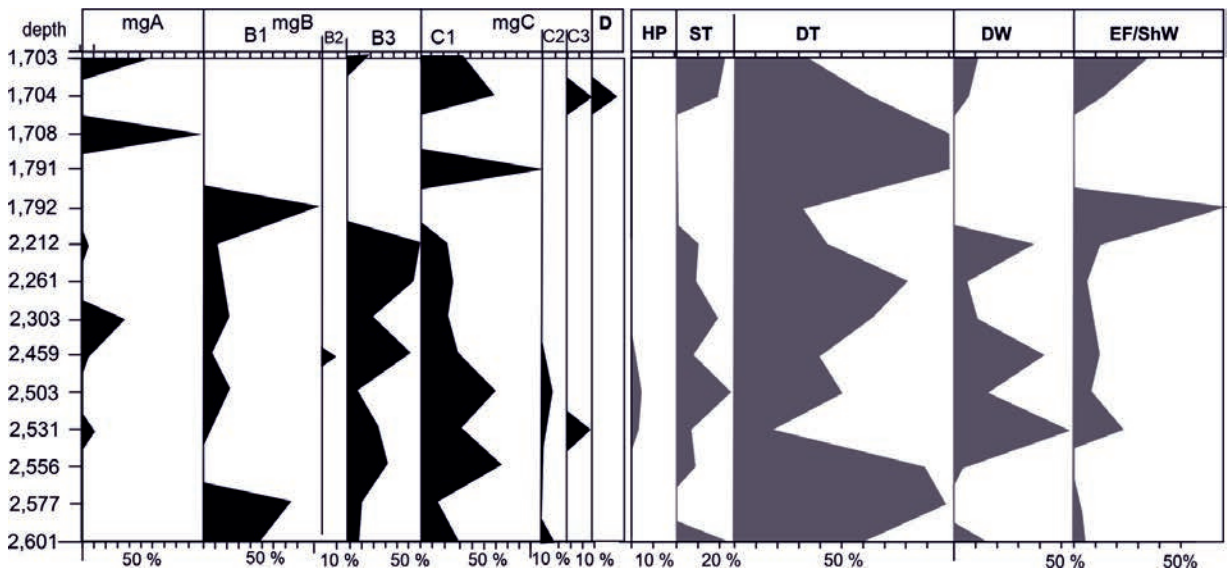

Fig. 7. Relative abundances of palaeoecologically significant groups of benthic foraminifera in samples from the Dubové-2 well. (Left) Morphogroups of agglutinated foraminifera adapted from Murray et al. (2011). (Right) Palaeoecological groups of benthic foraminifera based on Murray (2006) and other authors. Abbreviations: HP – high productivity; DT – dysoxia-tolerant taxa; DW – deep-water taxa; EF/ShW – epifaunal/shallow-water taxa.

Discussion

Well-scale depositional and chronostratigraphic interpretation

The interpretations below distinguish among evidence documented directly in core or thin section, age and environmental interpretations supported by fossil evidence, interpretations supported mainly by SP/RT logs or seismic geometry, and correlations inferred from the regional stratigraphic framework. Interpretations lacking direct core or fossil control are explicitly identified as tentative. The diagnostic observations and facies-association criteria are summarized in Tables 4 and 5; the following text focuses on their depositional and chronostratigraphic significance.

Špačince-4 well

Basal coarse-clastic interval, 3,356–3,259 m; C34–C33. The criteria summarized in Tab. 4 support high-energy, short-distance sediment transport within a proximal fan-delta or subaqueous debris-flow apron during early depocentre development, consistent with Blair (1999). The early lower Badenian age is regionally inferred.

Volcaniclastic interval, 3,259–3,125 m; C32–C30. The criteria summarized in Tab. 4 support volcaniclastic gravity-flow deposition in a fan-delta to subaqueous mass-flow system, consistent with Smith (1986). The massive zeolitized tuff may represent a subaqueous eruption-fed density current or secondary volcanoclastic deposit following the volcaniclastic model of Di Capua and Groppelli (2016) and Di Capua et al. (2023). Together, the interval indicates active volcanism, rapid sediment supply and early syn-rift subsidence. Its early lower Badenian age is regionally inferred.

Lower gravity-flow slope interval, 3,125–2,850 m; C29–C25. The criteria summarized in Tab. 4 indicate deposition from low-density turbidity currents and related fine-grained sediment-gravity flows in a slope to basin-floor setting, following the process framework of Talling et al. (2012). The abundance of agglutinated foraminifera and morphogroup ratios between ~3,003 and 2,849 m are compatible with upper- to middle-bathyal affinities only where the assemblages are plausibly in situ; taphonomic overprinting makes these palaeodepth estimates indicative rather than absolute. The FO of *Orbulina suturalis* and nannofossils including *Sphenolithus heteromorphus* and *Helicosphaera walbersdorfensis* constrain this interval to the lower Badenian (Langhian). The absence of reworked volcanic material within this interval suggests the waning and progressive burial of the volcanic centre. The presence of clasts derived from Eocene sandstones indicates predominantly sediment transport from the west, in contrast to the underlying and overlying volcanically dominated successions. High pyrite content in the heavy fraction, elevated relative S and detectable Mo, together with benthic taxa tolerant of low oxygen availability, are consistent with decreasing of oxygen in bottom waters during deposition of this interval.

Submarine channel-turbidite system, 2,850–2,150 m; C24–C16. The criteria summarized in Tab. 4 support episodic high-density sediment-gravity flows within a submarine channel system, alternating with lower-density turbidites and suspension settling, following the process criteria of Talling et al. (2012). The reappearance of a volcanic source within this interval may be explained in two ways: either by tectonically driven uplift and exhumation of the original volcanic center, and/or by renewed volcanic activity. Radioisotopic ages from volcanic material in the Kráľová-1 and Madunice-3 wells show that volcanic activity in this area began before 14.1 Ma and persisted until 13.83 Ma (Šarinová et al., 2021; Rybár et al., 2024). Consequently, the persistence of volcanic activity appears to represent the more plausible interpretation. The upward decrease in unstable clasts accompanied by an increasing proportion of quartz suggests progressive reworking of the material. Nannofossil assemblages with *S. heteromorphus* and *H. waltrans* support an NN5 lower Badenian (Langhian) age or younger.

Outer shelf-slope distal gravity-flow interval, 2,150–1,125 m; C15–C6. The criteria summarized in Tab. 4 support suspension-dominated outer-shelf to slope deposition with episodic distal gravity-flow or weak traction-current input, consistent with Talling et al. (2012). The occurrence of *Globorotalia bykovae* acme, small planktonic foraminiferal blooms, and *Bulimina-Bolivina*-dominated assemblages indicates an upper Badenian (lower Serravallian) age and is consistent with enhanced organic flux and locally reduced bottom- or pore-water oxygen availability, rather than providing a direct measure of water depth or redox state.

Shelf to marginal-marine interval, 1,125–625 m; C5–C1. No core from this interval was examined in the present study. Carbonized plant fragments and marine macrofauna reported by Gaža (1963), together with high-amplitude serrated SP and RT motifs, are consistent with progressive shallowing toward shelf to marginal-marine conditions. The interpretation remains tentative. The interval is regionally assigned to the upper Badenian, although a transition into the Sarmatian cannot be excluded. The systematic decrease in S values above a depth of approximately 905 m, approaching near-zero values, is consistent with a trend toward lower salinity. However, given the limitations of the dataset, this observation cannot be regarded as direct evidence of decreasing water salinity, although it may support the interpretation of a transition to a marginal-marine depositional setting.

Upper log-defined interval, 625–0 m. No core material or direct fossil control is available. High-amplitude serrated RT and medium-amplitude serrated SP patterns indicate variable clastic input. Shallow- to marginal-marine, deltaic and younger lacustrine–fluvial environments are inferred from the log character, seismic architecture and regional stratigraphic framework. The Sarmatian–Pannonian age assignment is therefore regionally inferred and tentative.

Dubové-2 well

Pre-Cenozoic basement interval, 3,000–2,780 m; C31–C24. Legacy lithological and log evidence summarized in Tab. 5 supports interpretation of this interval as Permian-Cretaceous pre-Cenozoic basement, with possible Hronic and/or Fatric nappe affinity based on Biela (1978) and Droppa et al. (2024). The high-amplitude symmetrical

Tab. 4
Facies associations of the. For explanations, see Tab. 2.

Depth/core	Analysed sample	Foraminiferal markers	Nannofossil markers	CPN zone	NN zone	Regional stage	Formation	Confidence	References
3,098–3,049 m; C29–C28	29/1–2/20; 29/1–2/80; 28/2/10; 28/2/80	No reliable zonal marker; poorly preserved agglutinated and benthic assemblages	Rare *Sphenolithus heteromorphus* and *Helicosphaera walbersdorfensis*; some specimens questionable	Not assigned	?NN5	lower Badenian, Langhian; tentative	Špačince Fm.	L–M:	
2,949–2,952 m; C26	26/1/60	*Orbulina suturalis*; *Saccammina grzybowskii*; *Dentoglobigerina altispira*	*Helicosphaera walbersdorfensis*; *H. carteri*; *Reticulofenestra pseudoumbilicus*	CPN7-8	?NN5	lower Badenian, Langhian	Špačince Fm.	M–H:	*Saccammina grzybowskii* FO: Cicha et al. (1998)
2,695–2,698 m; C21	21/1/90	Barren of diagnostic foraminifera	*Sphenolithus heteromorphus* and *Helicosphaera waltrans*	Not assigned	NN5	lower Badenian, Langhian / upper Badenian, lower Serravallian	Špačince/ Báhoň Fm.	H for NN zone	
2,298–2,303 m; C17	17/2/X	Reworked *Cassigerinella chipolensis*; no reliable in-situ foraminiferal marker	*Sphenolithus heteromorphus*;	Not assigned	NN5	lower Badenian, Langhian / upper Badenian, lower Serravallian	Špačince/ Báhoň Fm.	M:	
1,798–1,804 m; C12	12/1–2/X	Acme of *Globorotalia bykovae*; *Orbulina universa*; *Pappina neudorfensis*; *Bolivina dilatata*	*Coccolithus pelagicus* and ?*Calcidiscus pataecus*; no diagnostic zonal marker	CPN8, Bulimina/ Bolivina	Not assigned	upper Badenian, lower Serravallian	Báhoň Fm.	H for forams	*Globorotalia bykovae*; *Orbulina universa* – CPN8 (Gonera, 2013)
1,498–1,503 m; C9	9/1/X; 9/5/X	*Turborotalita quinqueloba*; *Globigerinella obesa*; *Bolivina dilatata brevis*	*Sphenolithus abies*; *R. pseudoumbilicus* > 7 µm; *Coronocyclus nitescens*; *Orthorhabdus rioi*;	Not assigned	NN6	upper Badenian, lower Serravallian	Báhoň Fm.	M–H	

Confidence and evidence codes: H – high confidence – directly observed in core and supported by fossil or independent evidence; M – moderate confidence – core-supported but age or environment depends partly on logs, seismic or regional correlation; L – low/tentative – no direct core or fossil control. C – core observation; P – petrography; F – fossil evidence; L – well logs; S – seismic evidence; R – regional correlation. Confidence may differ between process and age assignments.

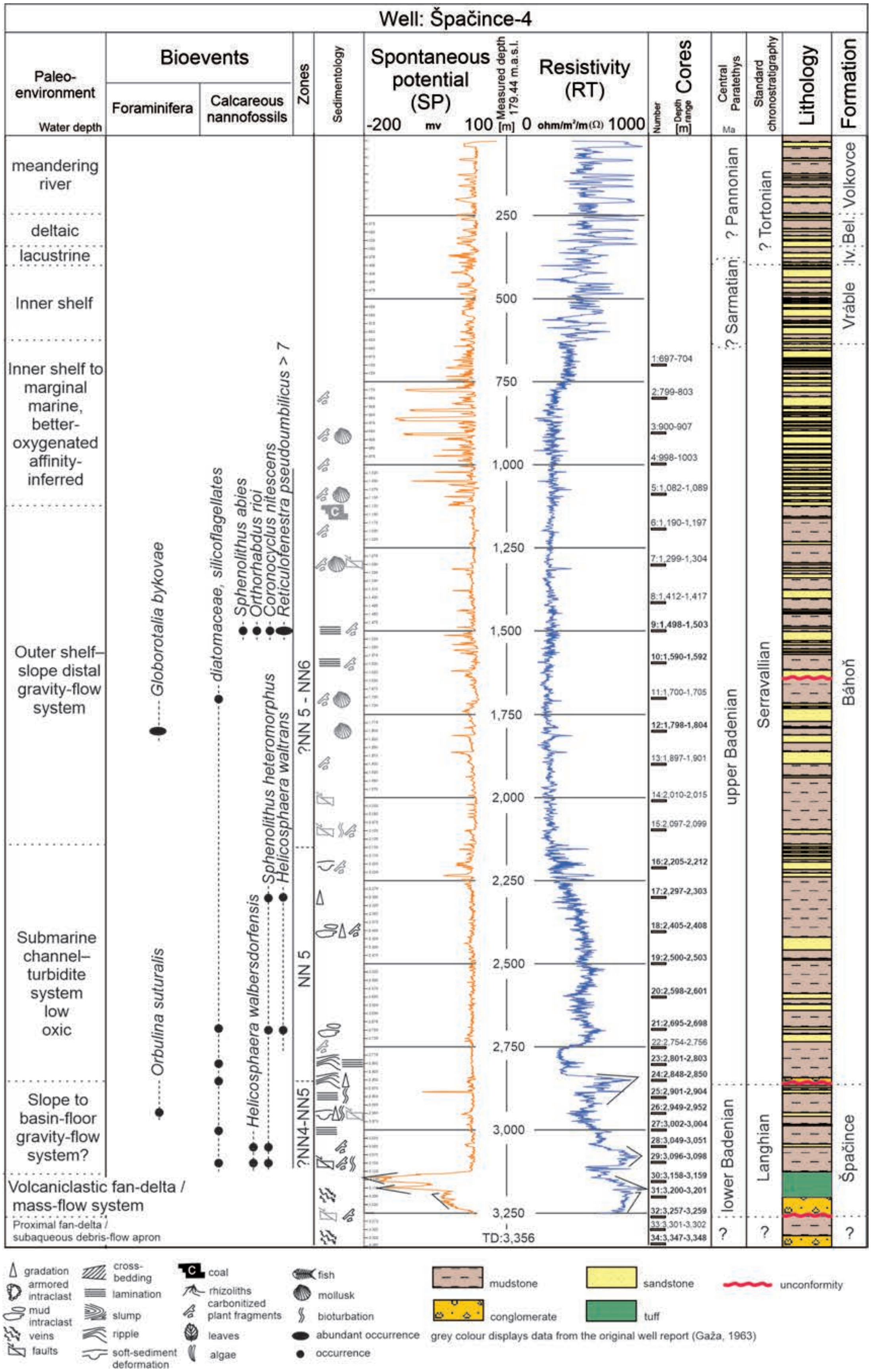
Well: Špačince-4
Paleo-environment
Water depth
Bioevents
Foraminifera
Calcareous nannofossils
Zones
Sedimentology
Spontaneous potential (SP)
-200 mv 100
Measured depth 179.44 m.a.s.l. [m]
Resistivity (RT)
0 ohm/m²/m(Ω) 1000
Number
Depth range [m]
Cores
Central Paratethys
Ma
Standard chronostratigraphy
Lithology
Formation
meandering river
deltaic
lacustrine
Inner shelf
Inner shelf to marginal marine, better-oxygenated affinity-inferred
Outer shelf–slope distal gravity-flow system
Submarine channel–turbidite system low oxic
Slope to basin-floor gravity-flow system?
Volcaniclastic fan-delta / mass-flow system
Proximal fan-delta / subaqueous debris-flow apron
Globorotalia bykovae
Orbulina suturalis
diatomaceae, silicoflagellates
Sphenolithus abies
Orthorhabdus rioi
Coronocyclus nitescens
Reticulofenestra pseudoumbilicus > 7
Sphenolithus heteromorphus
Helicosphaera waltrans
Helicosphaera walbersdorfensis
?NN 5 - NN6
NN 5
?NN4-NN5
250
500
750
1,000
1,250
1,500
1,750
2,000
2,250
2,500
2,750
3,000
3,250
TD:3,356
1:697-704
2:799-803
3:900-907
4:998-1003
5:1,082-1,089
6:1,190-1,197
7:1,299-1,304
8:1,412-1,417
9:1,498-1,503
10:1,590-1,592
11:1,700-1,705
12:1,798-1,804
13:1,897-1,901
14:2,010-2,015
15:2,097-2,099
16:2,205-2,212
17:2,297-2,303
18:2,405-2,408
19:2,500-2,503
20:2,598-2,601
21:2,695-2,698
22:2,754-2,756
23:2,801-2,803
24:2,848-2,850
25:2,901-2,904
26:2,949-2,952
27:3,002-3,004
28:3,049-3,051
29:3,096-3,098
30:3,158-3,159
31:3,200-3,201
32:3,257-3,259
33:3,301-3,302
34:3,347-3,348
? Pannonian
? Sarmatian
upper Badenian
lower Badenian
?
? Tortonian
Serravallian
Langhian
?
Volkovce
Iv.
Bel.
Vráble
Báhoň
Špačince
?
gradation
armored intraclast
mud intraclast
veins
faults
cross-bedding
lamination
slump
ripple
soft-sediment deformation
coal
rhizoliths
carbonitized plant fragments
leaves
algae
fish
mollusk
bioturbation
abundant occurrence
occurrence
mudstone
conglomerate
sandstone
tuff
unconformity
grey colour displays data from the original well report (Gaža, 1963)

Fig. 8. Integrated stratigraphic log of the Špačince-4 well showing palaeoenvironmental interpretation, fossil bioevents, and NN zones, sedimentary structures, SP and RT logs, core positions, lithology and formation assignments. Sarmatian and Pannonian assignments in intervals without direct fossil control are based on well-log, seismic and regional stratigraphic correlation and are considered tentative. Palaeodepth and redox interpretations derived from benthic assemblages are indicative and are subject to ecological, taphonomic and post-depositional controls.

to bell-shaped SP/RT responses are consistent with strong lithification and lithological contrasts following Rider and Kennedy (2011). A major hiatus separates the basement from the overlying Neogene succession.

Bioturbated sandstone interval, 2,780–2,720 m; C23. The criteria summarized in Tab. 5 support energetic shallow-marine shelf deposition involving tractional reworking and bioturbation, consistent with Howard and Reineck (1981). The symmetrical SP and funnel- to bell-shaped RT motifs indicate a discrete sand-rich body following Rider and Kennedy (2011). The precise shelf position remains uncertain, and gravity-influenced sand deposition cannot be excluded. The lower Badenian age is regionally inferred.

Sandy mudstone-muddy siltstone interval, 2,720–2,535 m; C22–C16. The criteria summarized in Tab. 5 support mixed suspension and distal gravity-flow deposition in a lower-energy outer-shelf to slope setting, following Talling et al. (2012). *Ciperoella ciperoensis* and rare ?*Helicosphaera ampliaperta* suggest a Karpatian to lower Badenian age, while the FO of *Saccammina grzybowskii* supports a Badenian (Langhian–lower Serravallian) assignment. The fossil evidence permits a Karpatian-Badenian assignment, whereas seismic and regional correlation favour a lower Badenian (Langhian) age.

Outer shelf-slope mudstone interval, 2,535–2,060 m; C15–C6. The criteria summarized in Tab. 5 support suspension-dominated outer-shelf to slope deposition, consistent with the fine-grained marine depositional framework of Macquaker et al. (2010). Agglutinated foraminiferal morphogroups from 2,503–2,212 m suggest bathyal-equivalent conditions if in situ, but sorting and dissolution may have modified the original assemblages. Benthic assemblages containing *Uvigerina macrocarinata*, *Lenticulina echinata*, *Pappina neudorfensis*, and *Uvigerina bellicostata*, together with *Sphenolithus heteromorphus*, constrain the interval mainly to Badenian (Langhian–lower Serravallian). Increased *Bulimina-Bolivina-Uvigerina* components are consistent with enhanced organic flux and locally reduced oxygen availability, but are not treated as direct depth indicators. The fossil evidence constrains the interval broadly to the Badenian, whereas seismic correlation favours a lower Badenian (Langhian) age.

Log-defined coarse-influx interval, 2,060–1,975 m. No core material is available from this interval. A pronounced high-amplitude symmetrical response is observed on both the SP and RT logs and is interpreted as a relatively sand-rich or coarse-clastic pulse. Possible explanations include a channelized sand body, a gravity-flow pulse or a sequence-stratigraphic surface associated with local tectonic or sediment-supply reorganization. Regional correlation suggests that the interval may correspond to the Langhian-Serravallian sea-level fall documented by Šarinová et al. (2021), but this event and age correlation remains tentative because it lacks direct core and fossil control.

Upper laminated mudstone and bioclastic interval, 1,975–470 m; C5–C1. The criteria summarized in Tab. 5 support low-energy marine suspension deposition interrupted by episodic reworked event beds, consistent with the event-bed framework of Kidwell et al. (1986). Fragmented macrofossils in shell-rich beds suggest storm, gravity-flow, or local mass-flow reworking. *Globorotalia bykovae*, *Globoturborotalita druryi*, and nannofossils near the NN5/NN6 boundary indicate an upper Badenian (lower Serravallian) age. The upward increase in shallow-water epiphytic forms suggests gradual shallowing in the upper part of the well.

Upper log-defined post-rift interval, < 470 m.

No core material or direct fossil control is available. High-amplitude serrated to symmetrical SP/RT responses indicate variable clastic input (Rider & Kennedy, 2011). Shallow-marine, marginal-marine, deltaic and younger lacustrine-fluvial environments are regionally inferred by comparison with the seismic architecture and published Danube Basin stratigraphy context (e.g., Šujan et al., 2016). The late syn-rift to post-rift interpretation and the Sarmatian-Pannonian age assignment are therefore tentative.

Seismic interpretation and well integration

The interpreted seismic profiles (lines 558_77, 558_86, 558a_86-Composite_1, and 554_77-Composite_2) image the structural framework and stratigraphic architecture of the Blatné sub-basin and adjacent areas (Figs. 10, 11). The profiles show a strongly asymmetric half-graben bounded by major listric normal faults that flatten downward and sole into the Paleozoic basement (Figs. 10, 11). This fault zone controlled Middle Miocene accommodation space and the thickness distribution of syn-rift deposits. The Paleozoic basement, together with overlying Late Paleozoic to Mesozoic cover and nappe units of the Inner Western Carpathians (Hók et al., 2014), forms a rugged

Tab. 5
Facies associations of the Dubové-2 well

Depth/core	Lithology	Structures	Fossils	SP/RT motif	Process/ environment; diagnostic criteria	Age	Confidence
3,000–2,780 m; C31–C24	Deformed shale, limestone, quartz arenite, sandstone and conglomerate	Tectonic deformation; primary structures poorly documented	No diagnostic fossil	High-amplitude symmetrical-bell SP/RT	Pre-Cenozoic basement; strong lithification, deformation and marked log contrasts	Permian–Cretaceous; possible Hronic/Fatric affinity	**M** Legacy C, L
2,780–2,720 m; C23	Massive-mottled bioturbated sandstone with carbonate clasts, quartz, feldspar, mica, chert, volcanics and glauconite	Massive, mottled and bioturbated	Bioclasts; glauconite	Symmetrical SP; funnel-bell RT	Energetic shallow-marine shelf; discrete sand body, bioturbation and probable tractional reworking. Exact shelf position uncertain	lower Badenian; regionally inferred	**M** C, L, R
2,720–2,535 m; C22–C16	Sandy mudstone-muddy siltstone; local very fine sandstone	Faint lamination, ripple/wavy fabric, diffuse grading, mud streaks, bioturbation	*G. ciperoensis, S. grzybowskii, rare H. ampliaperta*	Mainly serrated; minor high-amplitude excursions	Mixed suspension and distal gravity-flow deposition; fine grain size, diffuse grading and ripples; outer shelf-slope	lower Badenian favoured	**M–H** C, F, L, S
2,535–2,060 m; C15–C6	Mudstone, sandy mudstone and muddy siltstone	Massive-faintly laminated; bioturbated; coarse beds rare	Bivalves and micro-/macrofauna; agglutinated forams; *S. heteromorphus*	Serrated SP/RT	Suspension-dominated outer shelf-slope; mud-dominated facies and scarcity of tractional beds	Badenian; lower Badenian favoured by seismic correlation	**M–H** C, F, S
2,060–1,975 m; uncored	Unknown	Not observed	No fossil control	High-amplitude symmetrical SP/RT	Log-defined coarse/sand-rich influx; possible channel body, gravity-flow pulse or sequence surface	Tentative intra-Badenian event correlation	**L** L, R
1,975–470 m; C5–C1	Laminated mudstone-siltstone/fine sandstone; rare shell-rich beds	Parallel-wavy lamination; bioturbation; folding and partings	Fragmented macrofossils; *G. bykovae*, *G. druryi*; NN5/NN6 nannofossils	Low-amplitude serrated SP/RT	Low-energy suspension with reworked event beds; discrete shell-rich layers and fragmented fossils indicate storm/gravity-flow reworking; upward shallowing	upper Badenian	**H** C, F, L
< 470 m; uncored	No core	Not observed	No direct fossil control	High-amplitude serrated-symmetrical SP/RT	Shallow-/marginal-marine, deltaic and younger lacustrine-fluvial deposition; inferred from logs, seismic and regional stratigraphy	Sarmatian–Pannonian; regionally inferred	**L** L, S, R

Confidence and evidence codes: H – high confidence – directly observed in core and supported by fossil or independent evidence; M – moderate confidence – coresupported but age or environment depends partly on logs, seismic or regional correlation; L – low/tentative – no direct core or fossil control. C – core observation; P – petrography; F – fossil evidence; L – well logs; S, seismic evidence; R – regional correlation. Confidence may differ between process and age assignments.

Fig. 9. Integrated stratigraphic log of the Dubové-2 well showing palaeoenvironmental interpretation, fossil bioevents, CPN and NN zones, sedimentary structures, SP and RT logs, core positions, lithology and formation assignments. Sarmatian and Pannonian assignments in intervals without direct fossil control are based on well-log, seismic and regional stratigraphic correlation and are considered tentative. Palaeodepth and redox interpretations derived from benthic assemblages are indicative and are subject to ecological, taphonomic and post-depositional controls.

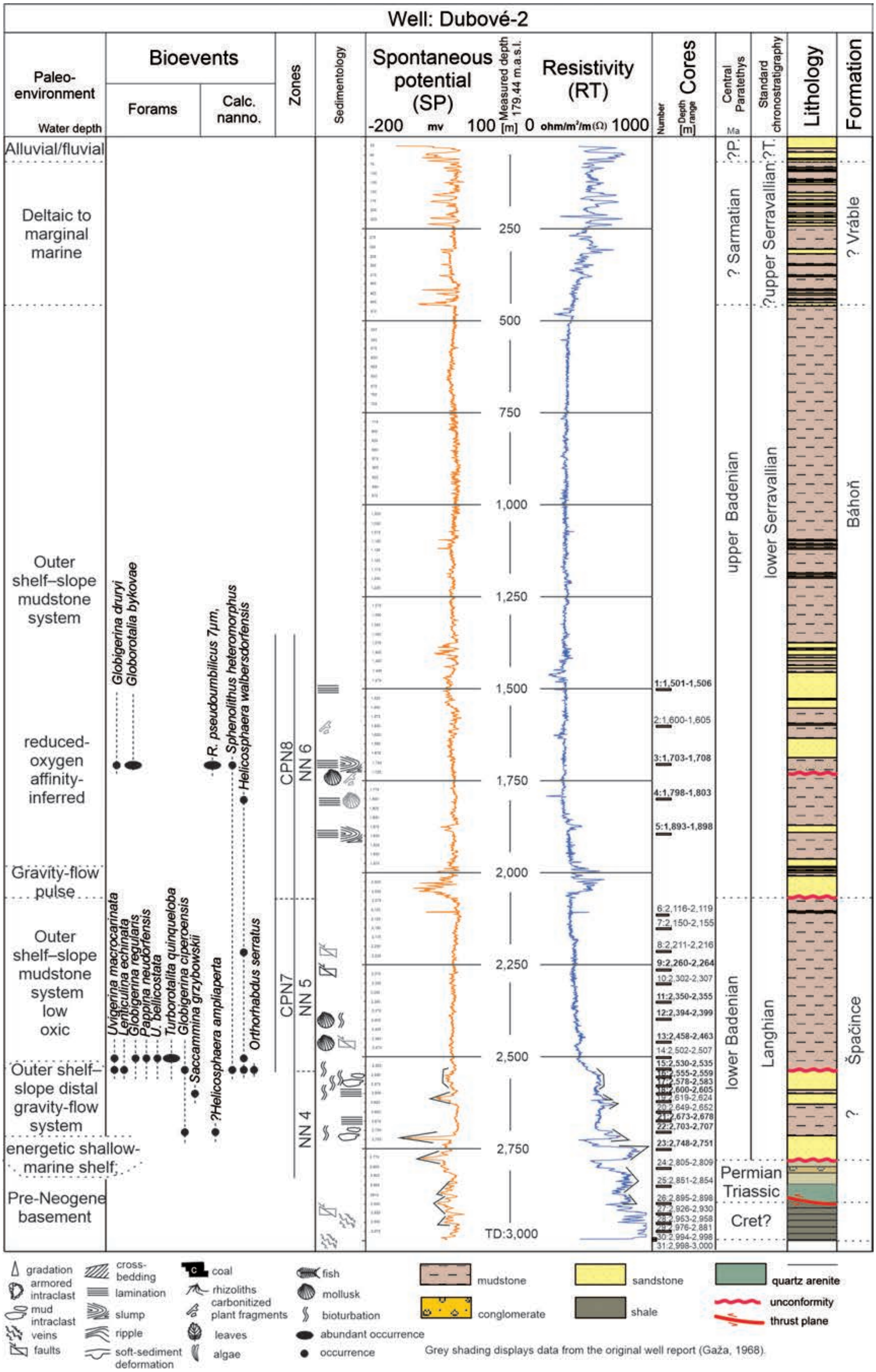
Well: Dubové-2
Paleo-environment
Water depth
Bioevents
Forams
Calc. nanno.
Zones
Sedimentology
Spontaneous potential (SP)
-200 mv 100
Measured depth 179.44 m.a.s.l. [m]
Resistivity (RT)
0 ohm/m²/m(Ω) 1000
Cores
Central Paratethys
Standard chronostratigraphy
Lithology
Formation
Alluvial/fluvial
Deltaic to marginal marine
Outer shelf–slope mudstone system
reduced-oxygen affinity-inferred
Gravity-flow pulse
Outer shelf–slope mudstone system low oxic
Outer shelf–slope distal gravity-flow system
energetic shallow-marine shelf
Pre-Neogene basement
Globigerina druryi
Globorotalia bykovae
R. pseudoumbilicus 7µm,
Sphenolithus heteromorphus
Helicosphaera walbersdorfensis
Uvigerina macrocarinata
Lenticulina echinata
Globigerina regularis
Pappina neudorfensis
U. bellicostata
Turborotalita quinqueloba
Globigerina ciperoensis
Saccammina grzybowskii
?Helicosphaera ampliaperta
Orthorhabdus serratus
CPN8
NN 6
CPN7
NN 5
NN 4
250
500
750
1,000
1,250
1,500
1,750
2,000
2,250
2,500
2,750
TD:3,000
1:1,501-1,506
2:1,600-1,605
3:1,703-1,708
4:1,798-1,803
5:1,893-1,898
6:2,116-2,119
7:2,150-2,155
8:2,211-2,216
9:2,260-2,264
10:2,302-2,307
11:2,350-2,355
12:2,394-2,399
13:2,458-2,463
14:2,502-2,507
15:2,530-2,535
16:2,555-2,559
17:2,578-2,583
18:2,600-2,605
19:2,619-2,624
20:2,649-2,652
21:2,673-2,678
22:2,703-2,707
23:2,748-2,751
24:2,805-2,809
25:2,851-2,854
26:2,895-2,898
27:2,926-2,930
28:2,953-2,958
29:2,976-2,881
30:2,994-2,998
31:2,998-3,000
?P.
? Sarmatian
upper Badenian
lower Badenian
?T.
?upper Serravallian
lower Serravallian
Langhian
Permian
Triassic
Cret?
? Vráble
Báhoň
Špačince
?
gradation
armored intraclast
mud intraclast
veins
faults
cross-bedding
lamination
slump
ripple
soft-sediment deformation
coal
rhizoliths
carbonitized plant fragments
leaves
algae
fish
mollusk
bioturbation
abundant occurrence
occurrence
mudstone
conglomerate
sandstone
shale
quartz arenite
unconformity
thrust plane
Grey shading displays data from the original well report (Gaža, 1968).

surface that deepens toward the basin centre (Figs. 10, 11). Thin and discontinuous Paleogene to Lower Miocene deposits are locally preserved on faulted structural highs in the northwestern part of the area, probably related to the Inner Carpathian Paleogene Basin and the Dobrá Voda Basin (Fig. 1). Above this surface, a thick Badenian syn-rift succession fills the half-graben. These deposits thicken toward the main fault zones and show inclined to divergent reflector geometries typical of growth strata (Gawthorpe et al., 1997; Figs. 10, 11). Their internal seismic facies are commonly chaotic to high-amplitude, locally corresponding to gravity-flow-dominated facies documented in the Špačince-4 and Dubové-2 wells (Figs. 8, 9). The lower Badenian (Langhian; Špačince Fm.; Vass, 2002) forms a laterally continuous seismic unit that thickens into the main depocentre and locally toward the eastern and southern basin margins, where large alluvial-fan to fan-delta bodies are preserved (Figs. 10, 11). Reflectors onlap intrabasinal highs and downlap toward the basin axis, consistent with active syn-rift deepening (Gawthorpe & Leeder, 2000). The overlying upper Badenian interval (lower Serravallian; Báhoň Fm.; Vass, 2002) is thicker and shows smoother reflector geometries, with downlap onto underlying units. This geometry indicates continued syn-rift subsidence (Gawthorpe & Leeder, 2000), but with higher sediment accumulation rates in line with models presented in Rybár et al. (2025). Above the Badenian growth packages, the seismic profiles show a regionally extensive, gently dipping package with limited thickness variation and common onlap onto the underlying syn-rift succession (Nøttvedt et al., 1995). This is overlain by comparatively subhorizontal reflectors that pond in the basin centre and thin across structural highs. Fault offsets also decrease upward. These seismic geometries indicate progressive basin infilling and waning fault activity. Based on correlation with the regional lithostratigraphic framework (e.g., Šujan et al., 2016), the onlapping package is inferred to represent the Sarmatian Vráble Formation (Vass, 2002), whereas the upper subhorizontal package is inferred to represent the Pannonian succession. The post-rift (Contreras et al., 1997) interpretation of the upper package is supported by its seismic geometry (Figs. 10, 11), but the detailed Sarmatian and Pannonian age assignments remain tentative because direct biostratigraphic control is absent.

Syn-rift sedimentation, marine deepening, and post-rift infilling of the Blatné sub-basin

The integrated well-log, core, micropalaeontological, and seismic data provide an opportunity to evaluate how the Blatné sub-basin (Fig. 1) evolved during the Badenian–Pannonian interval. The key question is how the variations between the Špačince-4 and Dubové-2 successions (Figs. 8, 9) reflect the timing of basin opening, changes in depositional environments, and the transition from syn-rift subsidence to post-rift infilling. We interpret these differences as the result of contrasting structural and depositional positions within an asymmetric Badenian half-graben, later modified by Sarmatian–Pannonian shallowing and progressive basin filling (Figs. 10, 11).

The principal advance of this study is the placement of the contrasting Špačince-4 and Dubové-2 successions within an asymmetric, fault-controlled half-graben and the reconstruction of their syn-rift to post-rift evolution. The basin-scale synthesis integrates core facies, biostratigraphy, palaeoecology, SP/RT logs and seismic architecture. Core and fossil evidence provide the strongest constraints, whereas interpretations based mainly on well logs, seismic geometry or uncored intervals are treated as lower confidence.

The contrasting successions in the Špačince-4 and Dubové-2 wells are interpreted as the result of different positions within the same evolving half-graben system. Špačince-4 contains a thicker syn-rift succession with basal coarse-clastic deposits, volcaniclastic material, and abundant gravity-flow facies (Figs. 2, 8), whereas Dubové-2 reaches pre-Neogene basement and contains a thinner Neogene succession beginning with sand-rich marine deposits (Figs. 3, 9). This interpretation is supported by the seismic architecture, which shows an asymmetric half-graben bounded by normal faults, syn-rift thickening toward fault zones, and growth-strata geometries (Figs. 10, 11). Špačince-4 was therefore probably located closer to an active depocentre and/or sediment-entry system, while Dubové-2 occupied a more marginal position, possibly near a structural high or fault block (Fig. 10). However, the observed contrast may also partly reflect local erosion, variable fault-block subsidence, or incomplete core and log control.

Lower Badenian deposition was strongly influenced by syn-rift subsidence and fault-controlled accommodation (Figs. 10, 11). In Špačince-4, basal paraconglomerates, volcanic conglomerate, zeolitized tuff, matrix-rich conglomerates, mudstone-siltstone intraclasts, chaotic fabrics, and locally erosive contacts (Fig. 2) indicate rapid sediment supply from unstable basin margins (Fig. 10). These core observations are consistent with the seismic evidence for growth strata and thickening toward normal faults (Fig. 10). Together, the data support deposition during active accommodation creation, short sediment-transport pathways, local volcanic input, and repeated gravity-flow activity along the margins of the developing depocentre. Nevertheless, the coverage of the volcanic sequence by non-volcanic sediments, followed by the renewed dominance of volcanic-derived material in the sedimentary record, suggests a temporary cessation of volcanic activity accompanied by burial of the volcanic centre. The sub-

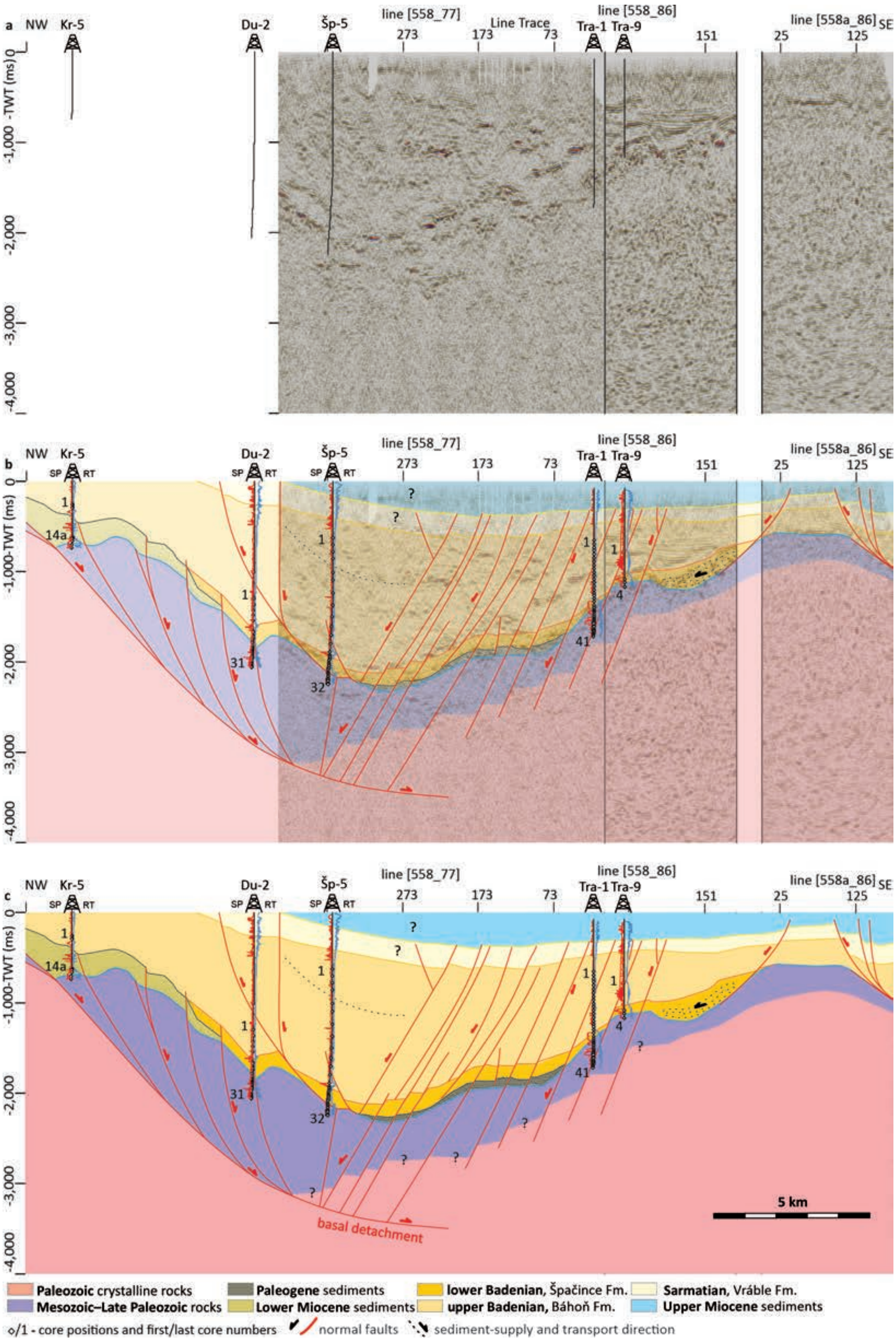

Fig. 10. Composite seismic profile 1 across the Blatné sub-basin. (a) Uninterpreted seismic data. (b) Seismic data with interpreted horizons, faults and well ties. (c) Geological interpretation. The Kr-5, Du-2, Šp-5, Tra-1 and Tra-9 wells provide lithological and well-log control. The vertical axis shows two-way travel time in milliseconds; horizontal distance and trace positions are indicated. Stratigraphic colours, faults, core positions and sediment-transport directions are explained in the legend. Sarmatian and Pannonian assignments in intervals without direct fossil control are based on seismic, well-log and regional stratigraphic correlation and are considered tentative.

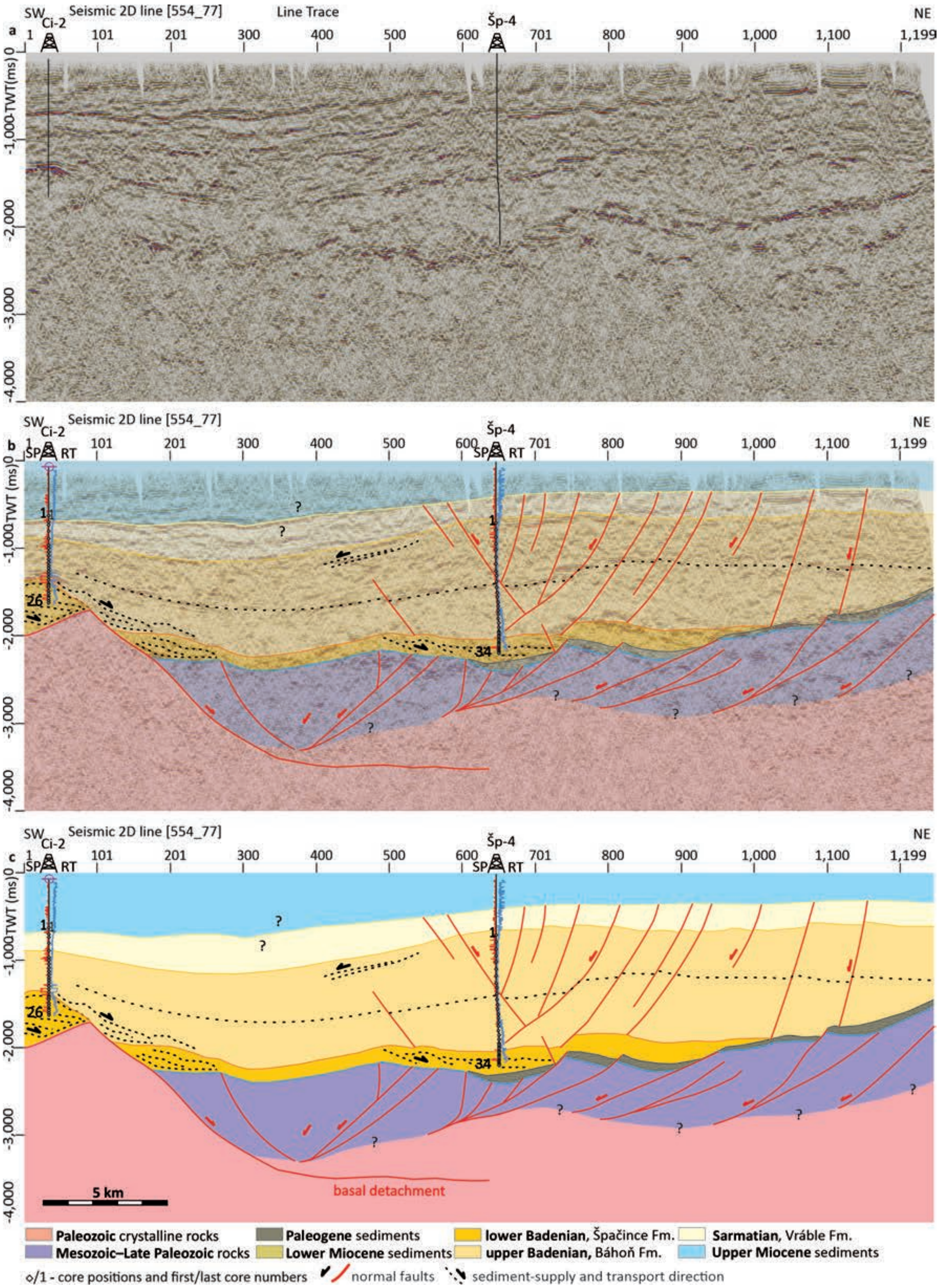

Fig. 11. Composite seismic profile 2, based on line 554_77, across the Blatné sub-basin. (a) Uninterpreted seismic data. (b) Seismic data with interpreted horizons, faults and well ties. (c) Geological interpretation. The Ci-2 and Šp-4 wells provide lithological and well-log control. The vertical axis is two-way travel time in milliseconds; the horizontal scale is displayed. Stratigraphic colours, faults and sediment-transport directions are explained in the legend. Sarmatian and Pannonian assignments without direct fossil control are tentative.

sequent reappearance of volcanic material is most plausibly linked to the renewal of volcanic activity. Although less likely, renewed exposure of the volcanic source due to tectonic uplift or a fall in sea level cannot be entirely excluded.

During the upper Badenian, marine environments developed unevenly across the sub-basin. Fine-grained mudstone-siltstone intervals, low-density turbidites, distal gravity-flow deposits, and suspension-dominated facies indicate outer shelf to shelf-slope deposition in both wells (Figs. 2, 3, 8, 9). Agglutinated foraminiferal morphogroups are compatible with bathyal-equivalent conditions in several intervals, particularly where they are interpreted as in situ (Figs. 4–7). However, poor preservation, dissolution, sorting, reworking, and the presence of damaged tests and moulds show that the original assemblages were locally modified. *Bulimina-Bolivina-Uvigerina*-rich assemblages indicate enhanced organic flux and locally reduced oxygenation rather than water depth alone, because benthic foraminiferal distributions are controlled mainly by food supply, organic flux, and oxygen availability (Jorissen et al., 1995; Van der Zwaan et al., 1999; Hayward et al., 2002). The occurrence of dysoxia-tolerant taxa, together with laminated fine-grained sediments, weak to variable bioturbation, phytoclasts, and terrestrial organic input, suggests enhanced organic flux to the sea floor. Reduced oxygenation may therefore reflect enhanced organic-matter production and export, limited ventilation caused by stratification or restricted circulation, and reduced oxygen exposure during rapid sediment accumulation and burial (Demaison & Moore, 1980; Hartnett et al., 1998; den Dulk et al., 2000; Rabalais et al., 2010). The XRF evidence is used only as supporting information. Elevated relative S and detectable Mo may be associated with reducing conditions, but they may also reflect early-diagenetic pyrite formation, organic-matter preservation, sediment mineralogy and provenance, or salinity effects (Tribovillard et al., 2006). Without independent mineralogical, organic-carbon or Fe-speciation data, bottom-water and pore-water redox conditions cannot be distinguished confidently.

The high-amplitude SP and RT interval in Dubové-2 between 2060 and 1975 m (Fig. 9) may represent a short-lived increase in sandier or coarser clastic input (Rider & Kennedy, 2011). It is tentatively correlated with the coarse gravity-flow interval in Špačince-4 at 2,848–2,850 m (Fig. 8) and may correspond to a sediment-supply pulse or sequence-stratigraphic surface (Coe et al., 2003) near the Langhian/Serravallian, intra-Badenian boundary, similar to the event described from the Madunice well series area by Šarinová et al. (2021) dated to ~13.8Ma. However, this interpretation remains tentative because the Dubové-2 interval is not core-confirmed (Fig. 9). Alternative explanations include local channelized deposition (Posamentier & Kolla, 2003), fault-controlled sediment routing within the evolving half-graben system (Gawthorpe & Leeder, 2000), or a lithological/log response that cannot be confidently interpreted as a basin-wide sequence-stratigraphic surface without additional regional correlation and stratal-geometry evidence (Catuneanu et al., 2009).

The well-based interpretation is consistent with the regional model of the Blatné sub-basin, where lower Badenian basin opening during Rift 1 was followed by continued upper Badenian syn-rift subsidence during Rift 2. The Sarmatian interval remains tectonically ambiguous. The upper subhorizontal seismic succession of Pannonian age is interpreted as post-rift, although its detailed correlation is only inferred by regional data (Šujan et al., 2016, 2021; Rybár et al., 2025). The lower Badenian coarse-clastic, volcaniclastic, and gravity-flow deposits in Špačince-4 (Figs. 2, 8) support the interpretation of an actively subsiding Blatné depocentre during the early syn-rift stage and are compatible with regional evidence for Middle Miocene volcanic activity around the Langhian/Serravallian transition (Šarinová et al., 2021; Rybár et al., 2024, 2025). The upper Badenian mudstone–siltstone and gravity-flow intervals can be correlated with the marine Špačince and Báhoň/Pozba formations, whereas the overlying shallowing trend and log-defined upper intervals are consistent with the transition toward the Vráble Formation and later Ivanka-Beladice-Volkovce depositional systems sensu Vass (2002) and Šujan et al. (2016, 2021). Compared with the Madunice well series on the eastern basin margin (Šarinová et al., 2021), the Špačince-4 and Dubové-2 data indicate that facies distribution was strongly controlled by local depocentre architecture, fault-block position, and sediment-entry pathways (Figs. 10, 11).

The volcaniclastic component may include reworked older or nearby deposits rather than exclusively primary eruptive input (Schneider et al., 2001), although contemporaneous volcanism is documented in neighbouring wells (Šarinová et al., 2021; Rybár et al., 2024). The resulting short transport pathways and localized sediment entry are consistent with fault-controlled sediment routing in extensional basins (Gawthorpe & Leeder, 2000).

Several limitations should be considered when evaluating this interpretation. Core coverage is incomplete, particularly in the upper parts of both wells (Figs. 2, 3, 8, 9), where depositional environments are inferred mainly from SP/RT log motifs, seismic architecture (Figs. 8–11), and regional stratigraphic correlation (Šujan et al., 2016, 2021; Šarinová et al., 2021; Rybár et al., 2024, 2025) rather than direct lithological evidence. Foraminiferal preservation is poor in several intervals, and agglutinated assemblages may have been affected by dissolution, sorting, and reworking; therefore, palaeodepth estimates based on these assemblages should be treated as indicative rather than absolute (Figs. 4–7). The Sarmatian and especially Pannonian interpretations are partly inferred from seismic and log-defined patterns calibrated by the regional lithostratigraphic framework. Similarly, the proposed correlation between the Dubové-2 high-amplitude interval at 2,060–1,975 m and the Špačince-4 coarse gravity-flow interval at 2,848–2,850 m remains tentative because the Dubové-2 interval lacks core confirmation (Figs. 8, 9).

The integrated data support a five-stage conceptual depositional model for the Badenian-Pannonian evolution of the Blatné sub-basin. (1) During the early lower Badenian, fault-controlled accommodation created a rapidly subsiding depocentre supplied by proximal coarse-clastic, debris-flow and fan-delta systems. This interval was also associated with volcanic activity, which ceased in this area at approximately 13.8 Ma (Šarinová et al., 2021). (2) Continued lower- to upper-Badenian subsidence was accompanied by marine transgression and deepening, leading to outer-shelf-slope to basin-floor deposition dominated by turbidites, debris flows and suspension settling, with locally bathyal-equivalent benthic assemblages where preservation permits and the assemblages are plausibly in situ. (3) During the late upper Badenian, high sediment supply and enhanced organic and nutrient flux accompanied fine-grained marine sedimentation and evidence consistent with locally reduced bottom- or pore-water oxygen availability. (4) A regionally inferred Sarmatian interval records progressive shallowing, increasing terrestrial influence and a transition towards restricted to marginal-marine environments. (5) The upper subhorizontal seismic package is tentatively correlated with the Pannonian and interpreted as a post-rift infill system characterized by aggradation and deltaic, lacustrine and fluvial sedimentation (Figs. 10, 11).

The present results refine, rather than replace, the established regional tectonic model of the Danube Basin. The integrated data show that lower Badenian basin opening was expressed differently within individual fault blocks: Špačince-4 records initial coarse-clastic and volcaniclastic deposition followed by marine deepening, whereas Dubové-2 records a thinner marine succession directly overlying pre-Neogene basement. Seismic growth strata and faultward thickening indicate that Špačince-4 occupied a position closer to the active depocentre, while Dubové-2 was situated closer to a structural high or marginal fault block. Nevertheless, the correlation of the uncored 2,060–1,975 m interval in Dubové-2 with the intra-Badenian coarse-clastic event, as well as the detailed age assignment of the Sarmatian–Pannonian upper intervals, remains tentative.

Conclusions

The integrated data support a conceptual depositional model for the Badenian-Pannonian evolution of the Blatné sub-basin:

(1) Calcareous nannofossils and foraminifera constrain the studied Neogene succession mainly to the lower–upper Badenian (Langhian–lower Serravallian). Nannofossil assemblages document NN4–NN6 zones, and planktonic foraminifera locally indicate CPN7–CPN8 zones. Important stratigraphic markers include *Orbulina suturalis, Globorotalia bykovae* acme, *?Helicosphaera ampliaperta, Sphenolithus heteromorphus, Sphenolithus abies* and large *Reticulofenestra pseudoumbilicus > 7 µm.* Sarmatian-Pannonian deposits are inferred mainly from upper log-defined and seismic intervals.

(2) Continued lower to upper Badenian subsidence was accompanied by marine transgression and deepening, leading to outer-shelf-slope to basin-floor deposition dominated by turbidites, debris flows and suspension settling, with locally bathyal-equivalent benthic assemblages where preservation permits and the assemblages are plausibly in situ.

(3) During the late upper Badenian, fine-grained marine sedimentation coincided with high sediment input, increased organic-matter and nutrient fluxes, and evidence of locally reduced oxygen availability in bottom waters or pore waters.

(4) Where sufficiently preserved and plausibly in situ, agglutinated-foraminiferal morphogroups are compatible with bathyal-equivalent conditions in several Badenian intervals. These palaeodepth estimates remain indicative because of dissolution, selective preservation, sorting, reworking and poor test preservation. *Bulimina-Bolivina-Uvigerina*-rich assemblages are consistent with enhanced organic flux and locally reduced bottom- or pore-water oxygen availability rather than water depth alone.

(5) Seismic profiles show that Badenian deposition occurred within an asymmetric half-graben controlled by listric normal faults soling into a low-angle detachment. Lower–upper Badenian (Langhian–lower Serravallian) strata thicken toward major faults and display growth-strata geometries, indicating active syn-rift subsidence. The onlap of an upper seismic package, regionally inferred to be Sarmatian (upper Serravallian), together with the upward decrease in fault offset, indicates waning tectonic activity, although it remains uncertain whether this package represents the final syn-rift stage or a transitional phase. The overlying subhorizontal reflectors are tentatively correlated with the Pannonian (Tortonian) succession and interpreted as evidence of major fault cessation and post-rift aggradation.

(6) The Špačince-4 and Dubové-2 successions represent different structural and depositional positions within the Blatné sub-basin. Špačince-4 was located closer to an active depocentre and sediment-entry system, whereas Dubové-2 occupied a more marginal position near a structural high or a fault block. This explains the contrast between the thick coarse-clastic/volcaniclastic gravity-flow succession in Špačince-4 and the thinner marine succession above basement in Dubové-2.

(7) Overall, the integrated data record a transition from Badenian fault-controlled syn-rift sedimentation to regionally inferred Sarmatian shallowing and tentatively correlated Pannonian post-rift deltaic-lacustrine-fluvial infilling.

Acknowledgements

We thank NAFTA, a. s., for access to its core repository and permission to sample. This work was supported by the APVV agency under contracts APVV-22-0523, APVV-23-0227 and APVV-20-0079, and by VEGA project 2/0106/23. The study was also funded by the EU NextGenerationEU through the Recovery and Resilience Plan for Slovakia under project 09I03-03-V04-00127. We also thank Schlumberger Ltd. for providing a Petrel software licence and Prof. M. Kováč for insightful comments. We are grateful to the editor and reviewer O. Pelech and to the anonymous reviewer.

References

Balázs, A., Matenco, L., Magyar, I., Horváth, F. & Cloetingh, S., 2016: The link between tectonics and sedimentation in back-arc basins: New genetic constraints from the analysis of the Pannonian Basin. *Tectonics*, 35, 6, 1526–1559. https://doi.org/10.1002/2015TC004109.

Balázs, A., Matenco, L., Granjeon, D., Alms, K., François, T. & Sztanó, O., 2021: Towards stratigraphic-thermo-mechanical numerical modelling: Integrated analysis of asymmetric extensional basins. *Global and Planetary Change*, 196, 103386. https://doi.org/10.1016/j.gloplacha.2020.103386.

Bartol, M., 2009: Middle Miocene calcareous nannoplankton of NE Slovenia (Western Central Paratethys). *Paleontološki institut Ivana Rakovca ZRC SAZU*, 1–136.

Biela, A., 1978: Hlboké vrty v zakrytých oblastiach Vnútorných Západných Karpát [Deep boreholes in the Western Carpathian basins.] *Regionálna geológia Západných Karpát*, 10, 1–224 (in Slovak).

Biely, A. (ed.), Bezák, V., Elečko, M., Kaličiak, M., Konečný, V., Lexa, J., Mello, J., Nemčok, J., Potfaj, M., Rakús, M., Vass, D., Vozár, J. & Vozárová, A., 1996: Explanation to the Geological Map of Slovakia 1 : 500 000. *Bratislava, Dionýz Štúr Publishers*, 76 pp. https://www.geology.sk/wp-content/uploads/documents/foto/geol_mapy_rep_500k1M/1995_Geologicka_mapa_SR_Biely_500000/pdf/Vysv_1-500_000_Explanation-to-geological-map-of-Slovakia_Biely.pdf.

Blair, T. C., 1999: Sedimentology of the debris-flow-dominated Warm Spring Canyon alluvial fan, Death Valley, California. *Sedimentology*, 46, 5, 941–965. https://doi.org/10.1046/j.1365-3091.1999.00260.x.

Boggs, S. Jr., 2006: Principles of sedimentology and stratigraphy, 4th edition. *Pearson Prentice Hall, Upper Saddle River*, 662 pp.

Bojar, A.-V., Barbu, V., Wojtowicz, A., Bojar, H.-P., Hałas, S. & Duliu, O. G., 2018: Miocene Slănic Tuff, Eastern Carpathians, Romania, in the context of the Badenian Salinity Crisis. *Geosciences*, 8, 2, 73. https://doi.org/10.3390/geosciences8020073.

Boltovskoy, E., 1976: Distribution of recent foraminifera of the South American region. In: Hedley, R. H. & Adams, C. G. (eds.): Foraminifera, Volume 2. *London, Academic Press*, 171–236.

Boltovskoy, E. & Wright, R., 1976: Recent Foraminifera. *W. Junk, The Hague*, 515 pp.

Bown, P. R. (ed.), 1998: Calcareous nannofossil biostratigraphy. *London, Chapman & Hall*, 315 pp.

Catuneanu, O., Abreu, V., Bhattacharya, J. P., Blum, M. D., Dalrymple, R. W., Eriksson, P. G., Fielding, C. R., Fisher, W. L., Galloway, W. E., Gibling, M. R., Giles, K. A., Holbrook, J. M., Jordan, R., Kendall, C. G. St. C., Macurda, B., Martinsen, O. J., Miall, A. D., Neal, J. E., Nummedal, D., Pomar, L., Posamentier, H. W., Pratt, B. R., Sarg, J. F., Shanley, K. W., Steel, R. J., Strasser, A., Tucker, M. E. & Winker, C., 2009: Towards the standardization of sequence stratigraphy. *Earth-Science Reviews*, 92, 1–2, 1–33. https://doi.org/10.1016/j.earscirev.2008.10.003.

Chernyshev, I. V., Konečný, V., Lexa, J., Kovalenker, V. A., Jeleň, S., Lebedev, V. A. & Goltsman, Y. V., 2013: K-Ar and Rb-Sr geochronology and evolution of the Štiavnica Stratovolcano, Central Slovakia. *Geologica Carpathica*, 64, 4, 327–360. https://doi.org/10.2478/geoca-2013-0023.

Cicha, I., Čtyroká, J., Jiříček, R. & Zapletalová, I., 1975: Principal biozones of the Late Tertiary in Eastern Alps and West Carpathians. In: Cicha, I. (ed.): Biozonal division of the Upper Tertiary basins of the Eastern Alps and West Carpathians. *Bratislava, IUGS Proceedings of the VI Congress*, 19–34.

Cicha, I., Rögl, F., Rupp, Ch. & Čtyroká, J., 1998: Oligocene-Miocene foraminifera of the Central Paratethys. *Abhandlungen der Senckenbergischen Naturforschenden Gesellschaft*, 549, 1–325.

Coe, A. L., Bosence, D. W. J., Church, K. D., Flint, S. S., Howell, J. A. & Wilson, R. C. L., 2003: The sedimentary record of sea-level change. *Cambridge, Cambridge University Press*, 288 pp.

Contreras, J., Scholz, C. H. & King, G. C. P., 1997: A model of rift basin evolution constrained by first-order stratigraphic observations. *Journal of Geophysical Research: Solid Earth*, 102, B4, 7673–7690. https://doi.org/10.1029/96JB03832.

Demaison, G. J. & Moore, G. T., 1980: Anoxic environments and oil source bed genesis. *Organic Geochemistry*, 2, 1, 9–31. https://doi.org/10.1016/0146-6380(80)90017-0.

Droppa, D. M., Hók, J., Rybár, S., Vojtko, R., Pelech, O., Kronome, B., Bielik, M., Šujan, M. & Šipka, F., 2024: Tectonic map of the pre-Cenozoic basement of the northern Danube Basin. *Geologica Carpathica*, 75, 6, 375–386. https://doi.org/10.31577/GeolCarp.2024.24.

den Dulk, M., Reichart, G. J., van Heyst, S., Zachariasse, W. J. & van der Zwaan, G. J., 2000: Benthic foraminifera as proxies of organic matter flux and bottom water oxygenation? A case history from the northern Arabian Sea. *Palaeogeography, Palaeoclimatology, Palaeoecology*, 161, 3–4, 337–359. https://doi.org/10.1016/S0031-0182(00)00074-2.

Di Capua, A. & Groppelli, G., 2016: Emplacement of pyroclastic density currents (PDCs) in a deep-sea environment: The Val d'Aveto Formation case, Northern Apennines, Italy. *Journal of Volcanology and Geothermal Research*, 328, 1–8. https://doi.org/10.1016/j.jvolgeores.2016.08.003.

Di Capua, A., De Rosa, R., Kereszturi, G., Le Pera, E., Rosi, M. & Watt, S. F. L., 2023: Volcanically-derived deposits and sequences: a unified terminological scheme for application in modern and ancient environments. *Geological Society, London, Special Publications*, 520, 11–27. https://doi.org/10.1144/SP520-2021-201.

Emery, D. & Myers, K. J., 1996: Sequence stratigraphy. *Oxford, Blackwell Science,* 297 pp. https://doi.org/10.1002/9781444313710.

Fischer, K. C. & Veeken, P., 2015: Seismic and sequence stratigraphy. *Montan Universität,* 112 pp.

Fodor, L., Balázs, A., Csillag, G., Dunkl, I., Héja, G., Jelen, B., Kelemen, P., Kövér, S., Németh, A., Nyíri, D., Selmeczi, I., Trajanova, M., Vrabec, M. & Vrabec, M., 2021: Crustal exhumation and depocenter migration from the Alpine orogenic margin towards the Pannonian extensional back-arc basin controlled by inheritance. *Global and Planetary Change*, 201, 103475. https://doi.org/10.1016/j.gloplacha.2021.103475.

Fordinál, K. & Elečko, M., 2000: Ripnianske súvrstvie – sladkovodné sedimenty sarmatu a spodného panónu rišňovskej priehlbiny. *Mineralia Slovaca*, 32, 1, 55–60.

Fusán, O., Biely, A., Ibrmajer, J., Plančár, J. & Rozložník, L., 1987: Basement of the Tertiary of the Inner Western Carpathians. *Bratislava, Geological Institute of Dionýz Štúr* (in Slovak).

Csibri, T., Rybár, S., Šarinová, K., Jamrich, M., Sliva, Ľ. & Kováč, M., 2018: Miocene fan delta conglomerates in the north-western part of the Danube Basin: provenance, paleoenvironment, paleotransport and depositional mechanisms. *Geologica Carpathica*, 69, 5, 467–482. https://doi.org/10.1515/geoca-2018-0027.

Gaža, B., 1963: Záverečná geologická správa o pionierskom vrte Špačince-4. Manuscript. Plavecký Štvrtok, Archive of Nafta.

Gaža, B., 1968: Záverečná geologická správa o pionierskom vrte Dubové-2. Manuscript. Plavecký Štvrtok, Archive of Nafta.

Gawthorpe, R. L., Sharp, I., Underhill, J. R. & Gupta, S., 1997: Linked sequence stratigraphic and structural evolution of propagating normal faults. *Geology*, 25, 9, 795–798. https://doi.org/10.1130/0091-7613(1997)025%3C0795:LSSASE%3E2.3.CO;2.

Gawthorpe, R. L. & Leeder, M. R., 2000: Tectono-sedimentary evolution of active extensional basins. *Basin Research*, 12, 3–4, 195–218. https://doi.org/10.1111/j.1365-2117.2000.00121.x.

Gonera, M., 2013: Globorotaliid intervals of the sub-evaporite Badenian, Middle Miocene, in the Upper Silesia Basin, Central Paratethys, Poland. *Geological Quarterly*, 57, 4, 757–768. https://doi.org/10.7306/gq.1125.

Grill, R., 1941: Stratigraphische Untersuchungen mit Hilfe von Mikrofaunen im Wiener Becken und den benachbarten Molasse-anteilen. *Öl und Kohle*, 37, 31, 595–602.

Harangi, S., Vaselli, O., Tonarini, S., Szabó, C., Harangi, R. & Coradossi, N., 1995: Petrogenesis of Neogene extension-related alkaline volcanic rocks of the Little Hungarian Plain Volcanic Field (Western Hungary). *Acta Vulcanologica,* 7, 2, 173–187.

Harangi, S. & Lenkey, L., 2007: Genesis of the Neogene to Quaternary volcanism in the Carpathian-Pannonian region: Role of subduction, extension, and mantle plume. In: Beccaluva, L., Bianchini, G. & Wilson, M. (eds.): Cenozoic volcanism in the Mediterranean area. *Geological Society of America Special Paper*, 418, 67–92. https://doi.org/10.1130/2007.2418(04).

Harangi, S., Seghedi, I. & Lukács, R., 2025: The Neogene--Quaternary volcanism of the Carpathian-Pannonian region: from initial plate tectonic models to quantitative petrogenetic explanations. In: Tari, G. C., Kitchka, A., Krézsek, C., Lučić, D., Markič, M., Radivojević, D., Sachsenhofer, R. F. & Šujan, M. (eds.): The Miocene Extensional Pannonian Superbasin, Volume 1: Regional Geology. *Geological Society, London, Special Publications*, 554 pp. https://doi.org/10.1144/SP554-2024-84.

Hartnett, H. E., Keil, R. G., Hedges, J. I. & Devol, A. H., 1998: Influence of oxygen exposure time on organic carbon preservation in continental margin sediments. *Nature,* 391, 572–575. https://doi.org/10.1038/35351.

Hayward, B. W., Neil, H., Carter, R., Grenfell, H. R. & Hayward, J. J., 2002: Factors influencing the distribution patterns of Recent deep-sea benthic foraminifera, east of New Zealand, Southwest Pacific Ocean. *Marine Micropaleontology*, 46, 1–2, 139–176. https://doi.org/10.1016/S0377-8398(02)00047-6.

Hohenegger, J., 2005: Estimation of environmental paleogradient values based on presence/absence data: A case study using benthic foraminifera for paleodepth estimation. *Palaeogeography, Palaeoclimatology, Palaeoecology,* 217, 115–130.

Hohenegger, J., Ćorić, S. & Wagreich, M., 2014: Timing of the Middle Miocene Badenian Stage of the Central Paratethys. *Geologica Carpathica*, 65, 1, 55–66. https://doi.org/10.2478/geoca-2014-0004.

Hók, J., Šujan, M. & Šipka, F., 2014: Tectonic division of the Western Carpathians: An overview and a new approach. *Acta Geologica Slovaca*, 6, 2, 135–143.

Hók, J., Kováč, M., Pelech, O., Pešková, I., Vojtko, R. & Králiková, S., 2016: The Alpine tectonic evolution of the Danube Basin and its northern periphery, southwestern Slovakia. *Geologica Carpathica*, 67, 5, 495–505. https://doi.org/10.1515/geoca-2016-0031.

Holcová, K., 1997: Can detailed sampling and taphonomical analysis of foraminiferal assemblages offer new data for paleoecological interpretations? *Revue de Micropaléontologie*, 40, 4, 313–329. https://doi.org/10.1016/S0035-1598(97)90664-4.

Holbourn, A., Kuhnt, W., Clemens, S., Prell, W. & Andersen, N., 2013: Middle to late Miocene stepwise climate cooling: Evidence from a high-resolution deep water isotope curve spanning 8 million years. *Paleoceanography*, 28, 1–12.

Horváth, F., 1995: Phases of compression during the evolution of the Pannonian Basin and its bearing on hydrocarbon exploration. *Marine and Petroleum Geology*, 12, 8, 837–844. https://doi.org/10.1016/0264-8172(95)98851-U.

Horváth, F., Bada, G., Szafián, P., Tari, G., Ádám, A. & Cloetingh, S., 2006: Formation and deformation of the Pannonian Basin: Constraints from observational data. In: Gee, D. G. & Stephenson, R. A. (eds.): European lithosphere dynamics. *Geological Society, London, Memoirs*, 32, 191–206.

Horváth, F., Musitz, B., Balázs, A., Végh, A., Uhrin, A., Nádor, A., Koroknai, B., Pap, N., Tóth, T. & Wórum, G., 2015: Evolution of the Pannonian Basin and its geothermal resources. *Geothermics*, 53, 328–352.

Howard, J. D. & Reineck, H.-E., 1981: Depositional facies of high-energy beach-to-offshore sequence: Comparison with low-energy sequence. *AAPG Bulletin*, 65, 5, 807–830. https://doi.org/10.1306/2F919B0C-16CE-11D7-8645000102C1865D.

Hrušecký, I., 1999: Central part of the Danube Basin in Slovakia: Geophysical and geological model in regard to hydrocarbon prospection. *Exploration Geophysics, Remote Sensing and Environment*, 6, 1, 2–55.

Hudáčková, N. H., Kováč, M., Ruman, A., Halásová, E., Jamrich, M., Kováčová, M., Rybár, S., Šujan, M. & Šarinová, K., 2018: Biostratigraphy and paleoenvironmental interpretation of the Špačince-4 and Dubové-2 wells. Unpublished technical report, Order No. 45045664, prepared for NAFTA a.s. GEMINI. *Bratislava, Association of the Faculty of Natural Sciences, Comenius University in Bratislava and PRICOM*, 35 pp.

Haunold, T. G., 1995: Zur Taxonomie, Systematik und stratigraphischen Bedeutung uvigerinider Foraminiferen im Neogen des Wiener Beckens und benachbarter Gebiete – 40 Jahre nach Papp & Turnowsky (1953). *Jahrbuch der Geologischen Bundesanstalt*, 138, 1, 67–87.

Jorissen, F. J., de Stigter, H. C. & Widmark, J. G. V., 1995: A conceptual model explaining benthic foraminiferal microhabitats. *Marine Micropaleontology*, 26, 1–4, 3–15. https://doi.org/10.1016/0377-8398(95)00047-X.

Karátson, D., Márton, E., Harangi, S., Józsa, S., Balogh, K., Pécskay, Z., Kovácsvölgyi, S., Szakmány, Gy. & Dulai, A., 2000: Volcanic evolution and stratigraphy of the Miocene Börzsöny Mountains, Hungary: An integrated study. *Geologica Carpathica*, 51, 5, 325–343.

Karátson, D., Oláh, I., Pécskay, Z., Márton, E., Harangi, S., Dulai, A., Zelenka, T. & Kósik, S., 2007: Miocene volcanism in the Visegrád Mountains, Hungary: An integrated approach to regional volcanic stratigraphy. *Geologica Carpathica*, 58, 6, 541–563.

Kidwell, S. M., Fürsich, F. T. & Aigner, T., 1986: Conceptual framework for the analysis and classification of fossil concentrations. *Palaios*, 1, 3, 228–238. https://doi.org/10.2307/3514687.

Killényi, E. & Šefara, J. (eds.), 1989: Pre-Tertiary basement contour map of the Carpathian Basin beneath Austria, Czechoslovakia and Hungary, 1:500,000. *Budapest, Eötvös Loránd Geophysical Institute of Hungary*.

Klučiar, T., Kováč, M., Vojtko, R., Rybár, S., Šujan, M. & Králiková, S., 2016: The Hurbanovo-Diósjenő Fault: A crustal-scale weakness zone at the boundary between the Central Western Carpathians and Northern Pannonian Domain. *Acta Geologica Slovaca*, 8, 1, 59–70.

Konečný, V., Kováč, M., Lexa, J. & Šefara, J., 2002: Neogene evolution of the Carpatho-Pannonian region: An interplay of subduction and back-arc diapiric uprise in the mantle. *EGS Stephan Mueller Special Publication Series*, 1, 105–123.

Kováč, M., Andreyeva-Grigorovich, A., Bajraktarević, Z., Brzobohatý, R., Filipescu, S., Fodor, L., Harzhauser, M., Nagymarosy, A., Oszczypko, N., Pavelić, D., Rögl, F., Saftić, B., Sliva, Ľ. & Studencka, B., 2007: Badenian evolution of the Central Paratethys Sea: Paleogeography, climate and eustatic sea-level changes. *Geologica Carpathica*, 58, 6, 579–606.

Kováč, M., Synak, R., Fordinál, K., Joniak, P., Tóth, C., Vojtko, R., Nagy, A., Baráth, I., Maglay, J. & Minár, J., 2011: Late Miocene and Pliocene history of the Danube Basin: inferred from development of depositional systems and timing of sedimentary facies changes. *Geologica Carpathica*, 62, 6, 519–534.

Kováčová, P. & Hudáčková, N., 2009: Late Badenian foraminifers from the Vienna Basin (Central Paratethys): stable isotope study and paleoecological implications. *Geologica Carpathica*, 60, 1, 59–70. https://doi.org/10.2478/v10096-009-0006-3.

Lexa, J., Seghedi, I., Szakács, A., Németh, K., Konečný, V., Pécskay, Z., Fülöp, A. & Kovacs, M., 2010: Neogene-Quaternary volcanic forms in the Carpathian-Pannonian region: A review. *Central European Journal of Geosciences*, 2, 3, 207–270. https://doi.org/10.2478/v10085-010-0024-5.

Lexa, J., Yi, K., Broska, I., Ciesielska, Z., Koděra, P., Kohút, M., Mathur, R., Prcúch, J., Szczerba, M., Uhlík, P. & Vojtko, R., 2025: Evolution of the Štiavnica Stratovolcano revisited: SHRIMP U-Th-Pb zircon dating of subvolcanic intrusions, caldera fill and B. Hodruša precious/base metal deposit (including Re/Os and K/Ar data). *Geologica Carpathica*, 76, 1–24. https://doi.org/10.31577/GeolCarp.2025.05.

Loeblich, A. R. & Tappan, H., 1992: Present status of foraminiferal classification. In: Takayanagi, Y. & Saito, T. (eds.): Studies in Benthic Foraminifera. *Tokai University Press*, 93–102.

Macquaker, J. H. S., Bentley, S. J. & Bohacs, K. M., 2010: Wave-enhanced sediment-gravity flows and mud dispersal across continental shelves: Reappraising sediment transport processes operating in ancient mudstone successions. *Geology*, 38, 10, 947–950. https://doi.org/10.1130/G31093.1.

Matenco, L. & Radivojević, D., 2012: On the formation and evolution of the Pannonian Basin: Constraints derived from the structure of the junction area between the Carpathians and Dinarides. *Tectonics*, 31, 6, TC6007. https://doi.org/10.1029/2012TC003206.

Mitchum, R. M. Jr. & Vail, P. R., 1977: Seismic stratigraphy and global changes of sea level. Part 6: Stratigraphic interpretation of seismic reflection patterns in depositional sequences. In: Payton, C. E. (ed.): Seismic Stratigraphy – Applications to Hydrocarbon Exploration. *AAPG Memoir*, 26, 135–144.

Murray, J. W., 2006: Ecology and applications of benthic foraminifera. *Cambridge, Cambridge University Press*, 426 pp. https://doi.org/10.1017/CBO9780511535529.

Murray, J. W. & Alve, E., 2011: The distribution of agglutinated foraminifera in NW European seas: Baseline data for the interpretation of fossil assemblages. *Palaeontologia Electronica*, 14, 2.

Murray, J. W., Alve, E. & Jones, B. W., 2011: A new look at modern agglutinated benthic foraminiferal morphogroups: Their value in palaeoecological interpretation. *Palaeogeography, Palaeoclimatology, Palaeoecology*, 309, 229–241. https://doi.org/10.1016/j.palaeo.2011.06.006.

Nalepka, D. & Walanus, A., 2003: Data processing in pollen analysis. *Acta Palaeobotanica*, 43, 1, 125–134.

Nichols, G., 2009: Sedimentology and stratigraphy. *Chichester, Wiley-Blackwell*, 432 pp.

Nováková, P., Rybár, S., Šarinová, K., Nagy, A., Hudáčková, N., Jamrich, M., Teodoridis, V., Kováčová, M., Šujan, M., Vlček, T. & Kováč, M., 2020: The late Badenian-Sarmatian, Serravallian, environmental transition calibrated by sequence stratigraphy, eastern Danube Basin, Central Paratethys. *Geologica Carpathica*, 71, 4, 291–313. https://doi.org/10.31577/GeolCarp.71.4.1.

Nøttvedt, A., Gabrielsen, R. H. & Steel, R. J., 1995: Tectonostratigraphy and sedimentary architecture of rift basins, with reference to the northern North Sea. *Marine and Petroleum Geology*, 12, 8, 881–901. https://doi.org/10.1016/0264-8172(95)98853-W.

Patruno, S., Hampson, G. J. & Jackson, C. A.-L., 2015: Quantitative characterisation of deltaic and subaqueous clinoforms. *Earth-Science Reviews*, 142, 79–119. https://doi.org/10.1016/j.earscirev.2015.01.004.

Pécskay, Z., Lexa, J., Szakács, A., Seghedi, I., Balogh, K., Konečný, V., Zelenka, T., Kovacs, M., Póka, T., Fülöp, A., Márton, E., Panaiotu, C. & Cvetković, V., 2006: Geochronology of Neogene magmatism in the Carpathian arc and intra-Carpathian area. *Geologica Carpathica*, 57, 6, 511–530.

Pellegrini, C., Patruno, S., Helland-Hansen, W., Steel, R. J. & Trincardi, F., 2020: Clinoforms and clinothems: Fundamental elements of basin infill. *Basin Research*, 32, 2, 187–205. https://doi.org/10.1111/bre.12446.

Piller, W. E., Harzhauser, M. & Mandic, O., 2007: Miocene Central Paratethys stratigraphy: Current status and future directions. *Stratigraphy*, 4, 151–168.

Płonka, K., 2017: Palaeontological analysis of Middle Miocene siltstones at Wiślica, Carpathian Foredeep, Poland. *Geologos*, 23, 29–43. https://doi.org/10.1515/logos-2017-0003.

Popov, S. V., Rögl, F., Rozanov, A. Y., Steininger, F. F., Shcherba, I. G. & Kováč, M. (eds.) 2004: Lithological-paleogeographic maps of Paratethys. 10 maps, Late Eocene to Pliocene. *Courier Forschungsinstitut Senckenberg*, 250, 1–46.

Posamentier, H. W. & Kolla, V., 2003: Seismic geomorphology and stratigraphy of depositional elements in deep-water settings. *Journal of Sedimentary Research*, 73, 3, 367–388. https://doi.org/10.1306/111302730367.

Rabalais, N. N., Díaz, R. J., Levin, L. A., Turner, R. E., Gilbert, D. & Zhang, J., 2010: Dynamics and distribution of natural and human-caused hypoxia. *Biogeosciences*, 7, 585–619. https://doi.org/10.5194/bg-7-585-2010.

Ratschbacher, L., Merle, O., Davy, P. & Cobbold, P., 1991a: Lateral extrusion in the Eastern Alps, Part 1: Boundary conditions and experiments scaled for gravity. *Tectonics*, 10, 2, 245–256. https://doi.org/10.1029/90TC02622.

Ratschbacher, L., Frisch, W., Linzer, H.-G. & Merle, O., 1991b: Lateral extrusion in the Eastern Alps, Part 2: Structural analysis. *Tectonics*, 10, 2, 257–271. https://doi.org/10.1029/90TC02623.

Rider, M. & Kennedy, M., 2011: The geological interpretation of well logs, 3rd edition. *Rider-French Consulting Limited*, 432 pp.

Rossi, V. M., Perillo, M. M., Steel, R. J. & Olariu, C., 2017: Quantifying mixed-process variability in shallow-marine depositional systems: What are sedimentary structures really telling us? *Journal of Sedimentary Research*, 87, 10, 1060–1074. https://doi.org/10.2110/jsr.2017.49.

Royden, L. H., Horváth, F. & Burchfiel, B. C., 1982: Transform faulting, extension, and subduction in the Carpathian-Pannonian region. *Geological Society of America Bulletin*, 93, 8, 717–725.

Royden, L. H., Horváth, F. & Rumpler, J. 1983: Evolution of the Pannonian Basin system: 1. Tectonics. *Tectonics*, 2, 1, 63–90. https://doi.org/10.1029/TC002i001p00063.

Rybár, S., Halásová, E., Hudáčková, N., Kováč, M., Kováčová, M., Šarinová, K. & Šujan, M., 2015: Biostratigraphy, sedimentology and paleoenvironments of the northern Danube Basin: Ratkovce-1 well case study. *Geologica Carpathica*, 66, 1, 51–67.

Rybár, S., Kováč, M., Šarinová, K., Halásová, E., Hudáčková, N., Šujan, M., Kováčová, M., Ruman, A. & Klučiar, T., 2016: Neogene changes in paleogeography, paleoenvironment and the provenance of sediment in the northern Danube Basin. *Bulletin of Geosciences*, 91, 2, 367–398.

Rybár, S. & Kotulová, J., 2023: Petroleum play types and source rocks in the Pannonian Basin, insight from the Slovak part of the Danube Basin. *Marine and Petroleum Geology*, 149, 106092. https://doi.org/10.1016/j.marpetgeo.2022.106092.

Rybár, S., Šarinová, K., Jourdan, F., Mayers, C. & Sliva, Ľ., 2024: Middle Miocene volcanic flare-up preceding and synchronous with the Langhian/Serravallian sea-level decline in the North Pannonian Basin: Insights from $^{40}Ar/^{39}Ar$ dating, geo-seismic analysis and 3D visualization of the subterranean Kráľová stratovolcano. *Basin Research*, 36, e12844. https://doi.org/10.1111/bre.12844.

Rybár, S., Nováková, P., Šarinová, K., Kotulová, J., Jourdan, F. & Mayers, C., 2025: Tectono-sedimentary evolution of the North Danube Basin: Insights from $^{40}Ar/^{39}Ar$ geochronology and basin modeling within the Pannonian back-arc system. *International Journal of Earth Sciences*, 114, 907–932. https://doi.org/10.1007/s00531-025-02524-z.

Sant, K., Kuiper, K. F., Rybár, S., Grunert, P., Harzhauser, M., Mandic, O., Jamrich, M., Šarinová, K., Hudáčková, N. & Krijgsman, W., 2020: $^{40}Ar/^{39}Ar$ geochronology using high sensitivity mass spectrometry: Examples from middle Miocene horizons of the Central Paratethys. *Geologica Carpathica*, 71, 2, 166–182. https://doi.org/10.31577/GeolCarp.71.2.5.

Schmid, S. M., Bernoulli, D., Fügenschuh, B., Matenco, L., Schefer, S., Schuster, R., Tischler, M. & Ustaszewski, K., 2008: The Alpine-Carpathian-Dinaridic orogenic system: Correlation and evolution of tectonic units. *Swiss Journal of Geosciences*, 101, 1, 139–183. https://doi.org/10.1007/s00015-008-1247-3.

Schneider, J.-L., Le Ruyet, A., Chanier, F., Buret, C., Ferrière, J., Proust, J.-N. & Rosseel, J.-B., 2001: Primary or secondary distal volcaniclastic turbidites: How to make the distinction? An example from the Miocene of New Zealand, Mahia Peninsula, North Island. *Sedimentary Geology*, 145, 1–2, 1–22. https://doi.org/10.1016/S0037-0738(01)00108-7.

Seghedi, I. & Downes, H., 2011: Geochemistry and tectonic development of Cenozoic magmatism in the Carpathian--Pannonian region. *Gondwana Research*, 20, 4, 655–672. https://doi.org/10.1016/j.gr.2011.06.009.

Smith, G. A., 1986: Coarse-grained nonmarine volcaniclastic sediment: Terminology and depositional process. *Geological Society of America Bulletin*, 97, 1, 1–10. https://doi.org/10.1130/0016-7606(1986)97<1:CNVSTA>2.0.CO;2.

Steininger, F. F. & Rögl, F., 1984: Paleogeography and palinspastic reconstruction of the Neogene of the Mediterranean and Paratethys. *Geological Society, London, Special Publications*, 17, 659–668.

Šarinová, K., Rybár, S., Halásová, E., Hudáčková, N., Jamrich, M., Kováčová, M. & Šujan, M., 2018: Integrated biostratigraphical, sedimentological and provenance analyses with implications for lithostratigraphic ranking: The Miocene Komjatice Depression of the Danube Basin. *Geologica Carpathica*, 69, 4, 382–409. https://doi.org/10.1515/geoca-2018-0023,

Šarinová, K., Hudáčková, N., Rybár, S., Jamrich, M., Jourdan, F., Frew, A., Mayers, C., Ruman, A., Subová, V. & Sliva, Ľ., 2021: ^{40}Ar/^{39}Ar dating and palaeoenvironments at the boundary of the early–late Badenian, Langhian–Serravallian, in the northwest margin of the Pannonian Basin System. *Facies*, 67, 29. https://doi.org/10.1007/s10347-021-00637-w.

Šujan, M., Braucher, R., Kováč, M., Bourlès, D., Rybár, S., Guillou, V. & Hudáčková, N., 2016: Application of the authigenic ^{10}Be/^{9}Be dating method to Late Miocene--Pliocene sequences in the northern Danube Basin, Pannonian Basin System: Confirmation of heterochronous evolution of sedimentary environments. *Global and Planetary Change*, 137, 35–53.

Šujan, M., Braucher, R., Rybár, S., Maglay, J., Nagy, A., Fordinál, K., Šarinová, K., Sýkora, M., Józsa, Š., ASTER Team & Kováč, M., 2018: Revealing the late Pliocene to Middle Pleistocene alluvial archive in the confluence of the Western Carpathian and Eastern Alpine rivers: ^{26}Al/^{10}Be burial dating from the Danube Basin (Slovakia). *Sedimentary Geology*, 377, 131–146. https://doi.org/10.1016/j.sedgeo.2018.10.001.

Šujan, M., Rybár, S., Kováč, M., Bielik, M., Majcin, D., Minár, J., Plašienka, D., Nováková, P. & Kotulová, J., 2021: The polyphase rifting and inversion of the Danube Basin revised. *Global and Planetary Change*, 196, 103375. https://doi.org/10.1016/j.gloplacha.2020.103375.

Šujan, M., Šarinová, K., Hók, J., Vlček, T., Ruman, A., Jamrich, M., Kováčová, M., Droppa, D. M., Fordinál, K., Nagy, A., Moravcová, M., Sztanó, O. & Kováč, M., 2026: Miocene to Quaternary evolution of the northern Danube Basin: a review of geodynamics, depositional systems and stratigraphy. *Geological Society, London, Special Publications*, 554, SP554-2024-66. https://doi.org/10.1144/SP554-2024-66.

Sztanó, O. & Tari, G., 1993: Early Miocene basin evolution in northern Hungary: Tectonics and eustasy. *Tectonophysics*, 226, 1–4, 485–502.

Sztanó, O., Kováč, M., Magyar, I., Šujan, M., Fodor, L., Uhrin, A., Rybár, S., Csillag, G. & Tőkés, L., 2016: Late Miocene sedimentary record of the Danube/Kisalföld Basin: Interregional correlation of depositional systems, stratigraphy and structural evolution. *Geologica Carpathica*, 67, 6, 525–542. https://doi.org/10.1515/geoca-2016-0033.

Talling, P. J., Masson, D. G., Sumner, E. J. & Malgesini, G., 2012: Subaqueous sediment density flows: Depositional processes and deposit types. *Sedimentology*, 59, 7, 1937–2003. https://doi.org/10.1111/j.1365-3091.2012.01353.x.

Tari, G., Horváth, F. & Rumpler, J., 1992: Styles of extension in the Pannonian Basin. *Tectonophysics*, 208, 1–3, 203–219. https://doi.org/10.1016/0040-1951(92)90345-7.

Tari, G., Báldi, T. & Báldi-Béke, M., 1993: Paleogene retroarc flexural basin beneath the Neogene Pannonian Basin: A geodynamic model. *Tectonophysics*, 226, 3–4, 433–456. https://doi.org/10.1016/0040-1951(93)90133-5.

Tari, G., Bada, G., Beidinger, A., Csizmeg, J., Danišik, M., Gjerazi, I., Grasemann, B., Kováč, M., Plašienka, D., Šujan, M. & Szafián, P., 2021: The connection between the Alps and the Carpathians beneath the Pannonian Basin: Selective reactivation of Alpine nappe contacts during Miocene extension. *Global and Planetary Change*, 197, 103401. https://doi.org/10.1016/j.gloplacha.2020.103401.

Tribovillard, N., Algeo, T. J., Lyons, T. W. & Riboulleau, A., 2006: Trace metals as paleoredox and paleoproductivity proxies: An update. *Chemical Geology*, 232, 1–2, 12–32. https://doi.org/10.1016/j.chemgeo.2006.02.012.

Vass, D., 2002: Litostratigrafia Západných Karpát: neogén a budínsky paleogén [Lithostratigraphy of the Western Carpathians: Neogene and Budín Paleogene sediments]. *Bratislava, Štátny geologický ústav Dionýza Štúra*, 202 pp.

Van der Zwaan, G. J., Duijnstee, I. A. P., den Dulk, M., Ernst, S. R., Jannink, N. T. & Kouwenhoven, T. J., 1999: Benthic foraminifers: Proxies or problems? A review of paleoecological concepts. *Earth-Science Reviews*, 46, 1–4, 213–236. https://doi.org/10.1016/S0012-8252(99)00011-2.

Wade, B. S., Pearson, P. N., Berggren, W. A. & Pälike, H., 2011: Review and revision of Cenozoic tropical planktonic foraminiferal biostratigraphy and calibration to the geomagnetic polarity and astronomical time scale. *Earth-Science Reviews*, 104, 1–3, 111–142. https://doi.org/10.1016/j.earscirev.2010.09.003.

Wijbrans, J., Németh, K., Martin, U. & Balogh, K., 2007: ^{40}Ar/^{39}Ar geochronology of Neogene phreatomagmatic volcanism in the western Pannonian Basin, Hungary. *Journal of Volcanology and Geothermal Research*, 164, 4, 193–204. https://doi.org/10.1016/j.jvolgeores.2007.05.009.

Young, J. R., 1998: Neogene. In: Bown, P. R. (ed.): Calcareous Nannofossil Biostratigraphy. *British Micropalaeontological Society Publications Series, Chapman & Hall*, 225–265.

Young, J. R., Bown, P. R. & Lees, J. A., 2022: Nannotax3 website. *International Nannoplankton Association*. Accessed 20 July 2026. https://www.mikrotax.org/Nannotax3.

Vývoj blatnianskej priehlbiny počas bádenu až panónu (lang – tortón) v severozápadnej časti Dunajskej panvy (centrálna Paratetýda): integrované biostratigrafické, faciálne a seizmické údaje z vrtov Špačince-4 a Dubové-2

Miocénny vývoj severozápadnej časti centrálnej Paratetýdy ovplyvňovala zaoblúková extenzia spojená s vývojom alpsko-karpatského orogénu a laterálnym únikom megajednotky ALCAPA (Royden et al., 1983; Tari et al., 1992; Schmid et al., 2008). V tomto geodynamickom prostredí vznikol panónsky panvový systém ako sústava synriftových depocentier charakterizovaných rýchlou subsidenciou, vysokou rýchlosťou sedimentácie a vulkanickou aktivitou. Dunajská panva predstavuje jedno z hlavných depocentier tohto systému. Jej severozápadná časť vrátane blatnianskej priehlbiny zachováva hrubú miocénnu sedimentárnu sukcesiu, ktorá dokumentuje prechod od synriftovej extenzie k postriftovej termálnej subsidencii. Regionálny model extenzného vývoja Dunajskej panvy vrátane viacfázového riftingu a následnej postriftovej subsidencie je v súčasnosti dobre zdokumentovaný (Hók et al., 2016; Šujan et al., 2021, 2026). Menej objasnený však zostáva jeho lokálny prejav v jednotlivých tektonických blokoch blatnianskej priehlbiny. Otázky sa týkajú najmä prechodu od proximálnej hruboklastickej a vulkanoklastickej sedimentácie k jednoznačne morským podmienkam, ako aj laterálnej korelácie a priestorovej architektúry bádenských gravitačných sedimentov medzi skúmanými vrtmi a priľahlými časťami priehlbiny. Táto štúdia prináša integrované vyhodnotenie hlbokých vrtov Špačince-4 a Dubové-2. Nadväzuje na predchádzajúcu biostratigrafickú správu (Hudáčková et al., 2018), ktorú významne rozširuje o podrobný sedimentologický a seizmostratigrafický výskum a o koreláciu s publikovanými údajmi absolútneho datovania. Analýza zahŕňa biostratigrafiu vápnitého nanoplanktónu a planktonických a bentických foraminifer, palynologické údaje, sedimentologický opis vrtných jadier a interpretáciu karotážnych záznamov a seizmických profilov. Cieľom štúdie je: 1. spresniť biostratigrafické členenie miocénnej sukcesie pomocou viacerých skupín mikrofosílií, 2. rekonštruovať sedimentárne prostredie a faciálnu architektúru, 3. posúdiť, či rozdiely medzi sukcesiami vo vrtoch Špačince-4 a Dubové-2 odrážajú ich odlišnú pozíciu v rámci tektonicky kontrolovaného halfgrabenu blatnianskej priehlbiny.

Biostratigrafické údaje zaraďujú prevažnú časť skúmanej neogénnej sukcesie do spodného až vrchného bádenu, teda do langu až spodného seravalu. Asociácie vápnitého nanoplanktónu dokumentujú zóny NN4 – NN6 a planktonické foraminifery miestami zóny CPN7 – CPN8. Sarmatské a panónske sedimenty boli identifikované predovšetkým na základe karotážnych záznamov, seizmickej geometrie a regionálnych korelácií. Vrt Špačince-4 zachytáva hrubú bádenskú synriftovú sukcesiu. Bazálne parakonglomeráty, vulkanické konglomeráty a zeolitizované tufy prechádzajú smerom nahor do pieskovcov, konglomerátov a laminovaných ílovcov a prachovcov. Tieto sedimenty dokumentujú proximálny prínos hruboklastického materiálu, vulkanoklastickú sedimentáciu, úlomkotoky, turbiditné prúdy a distálnu sedimentáciu zo suspenzie. Vrt Dubové-2 dosahuje predneogénne podložie a obsahuje tenšiu neogénnu sukcesiu, tvorenú najmä bioturbovanými pieskovcami, piesčitými ílovcami, prachovcami a jemnozrnnými sedimentmi vonkajšieho šelfu až svahu, ktoré sú miestami prerušované gravitačnými alebo preplavenými bioklastickými polohami. Geoseizmické profily zobrazujú blatniansku priehlbinu ako asymetrický halfgraben ohraničený listrickými poklesovými zlomami, ktoré sa smerom do hĺbky napájajú na nízkouhlovú plochu odlepenia (*detachment*). Bádenské sedimenty hrubnú smerom k hlavným zlomom a vytvárajú typickú geometriu syntektonických rastových vrstiev. Mladšie, sarmatské sedimenty na tieto telesá nasadajú a dokumentujú postupné zoslabovanie tektonickej aktivity. Subhorizontálne panónske reflexy zodpovedajú postriftovému vypĺňaniu panvy deltovými, jazernými a fluviálnymi sedimentmi. Rozdiely medzi skúmanými vrtmi sú výsledkom ich odlišnej pozície v rámci toho istého polpriekopového systému. Vrt Špačince-4 sa nachádza bližšie k aktívnemu depocentru a k hlavným prívodným trasám sedimentov, zatiaľ čo vrt Dubové-2 leží v okrajovej polohe v blízkosti štruktúrnej elevácie alebo vyzdvihnutého zlomového bloku. Integrované výsledky tak spresňujú lokálnu chronostratigrafickú a tektonicko-sedimentárnu architektúru blatnianskej priehlbiny bez toho, aby menili zavedený regionálny model zaoblúkového extenzného vývoja Dunajskej panvy.

Doručené / Received: 1. 6. 2026
Prijaté na publikovanie / Accepted: 15. 7. 2026

Electronic supplementary material available online: https://www.geology.sk/mineralia/

Supplementary	Table S1. Summary of datasets used in this study
Appendix 1.	Foraminifera from the Špačince-4 well
Appendix 2.	Foraminifera from the Dubové-2 well
Appendix 3.	Complete Špačince-4 handheld-XRF dataset
Appendix 4a.	Nannofossil sample data from the Špačince-4 well
Appendix 4b.	Nannofossil sample data from the Dubové-2 well